Published in final edited form as:

Annu Rev Biochem. 2009 ; 78: 673–699. doi:10.1146/annurev.biochem.78.080207.092132.

Proton-Coupled Electron Transfer in Biology: Results from Synergistic Studies in Natural and Model Systems

Steven Y. Reece and **Daniel G. Nocera**

Department of Chemistry, Massachusetts Institutes of Technology, Cambridge, Massachusetts 02139-4307

Daniel G. Nocera: nocera@mit.edu

Abstract

Proton-coupled electron transfer (PCET) underpins energy conversion in biology. PCET may occur with the unidirectional or bidirectional transfer of a proton and electron and may proceed synchronously or asynchronously. To illustrate the role of PCET in biology, this review presents complementary biological and model systems that explore PCET in electron transfer (ET) through hydrogen bonds [azurin as compared to donor-acceptor (D–A) hydrogen-bonded networks], the activation of C–H bonds [alcohol dehydrogenase and soybean lipoxygenase (SLO) as compared to Fe(III) metal complexes], and the generation and transport of amino acid radicals [photosystem II (PSII) and ribonucleotide reductase (RNR)as compared to tyrosine-modified photoactive Re(I) and Ru(II) complexes]. In providing these comparisons, the fundamental principles of PCET in biology are illustrated in a tangible way.

Keywords

amino acid radical; lipoxygenase; photosystem II; ribonucleotide reductase; tyrosine

INTRODUCTION

Proton-coupled electron transfer is a fundamental mechanism in biology. Enzymes often rely on the coupling of electrons and protons to affect primary metabolic steps involving charge transport and catalysis (1). Without the coupling of the proton and electron, many processes in biology would not be possible. For instance, consider the oxidation of tyrosine. The electron and proton must transfer in a concerted fashion if high energy intermediates are to be avoided. If the electron were to transfer in the absence of proton transfer, then the very strong acid $TyrOH^{\bullet+}$ ($pK_a = -\log K_a = -2$, where K_a is the acidity constant) is produced. To do so, a very oxidizing potential is needed (E = 1.46 V vs NHE). The high-energy pathways are avoided if the electron and proton transfer together. In this case, the $TyrO^{\bullet}$ radical is produced, and the high-energy process of first removing an electron (or, vice versa, first removing a proton) is circumvented. As illustrated in this discussion of tyrosine, PCET

DISCLOSURE STATEMENT

The authors are not aware of any affiliations, memberships, funding, or financial holdings that might be perceived as affecting the objectivity of this review.

combines redox and acid/base chemistry. The dual particle nature of proton-coupled electron transfer (PCET) (2–4) introduces mechanistic complexities not encountered in simple electron transfer (ET) reactions.

The concept of a proton and electron coupling has been long known in a thermodynamic sense. Consider the diagram developed by Pourbaix (5) in the 1950s to account for the pH dependency of a redox couple. In subsequent years, the kinetics of proton-electron coupling was inferred from free-energy relations for reactant-to-product conversions. The coupling of the proton to an electron was also in evidence from the kinetic isotope effects (KIEs) of observed rate constants. In 1949, Westheimer (6) identified the coupling of the proton to a redox event via a KIE for the oxidation of alcohols by chromic acid. KIEs subsequently became a standard method of analysis for enzymatic, organic, and inorganic reactions involving the proton and electron (7). In the early 1990s, attention turned toward isolating the PCET event and directly measuring the kinetics of the reaction, enabled by the development of hydrogen-bonded donor-acceptor (D–A) complexes (2, 8). With these measurements, a formalism for the PCET reaction began to appear (9, 10).

A PCET reaction is represented by the parallelogram scheme shown in Figure 1. Separate solvent coordinates, z_e and z_p, which account for the electron and the proton, respectively, define a two-dimensional coordinate space for the PCET reaction. These solvent coordinates are analogous to the single solvent coordinates employed in ET or proton transfer (PT) reactions, and as such, they are parametric in the distance coordinates of the electron and proton. In this representation, a family of paths describes PCET. Stepwise PT and ET reactions occur along the edges of Figure 1, and PCET includes the entire space within the parallelogram. The two regimes (edges and area within the two-coordinate space) are clearly distinct. The PCET mechanism is defined by a single transition state, with no intermediate states populated along the reaction coordinate; PCET is thus concerted, but the electron and proton events can be asynchronous or synchronous. In a stepwise mechanism, an intermediate is formed, and there are two distinct rate constants for the forward reaction and two separate transition states. Stepwise ET/PT or PT/ET can, in principle, be broken down and treated experimentally and theoretically as separate ET and PT events. Like any series of reactions, the rate-limiting rule applies:

$$k_{\mathrm{ET/PT}} = \frac{k_{\mathrm{ET}} k_{\mathrm{PT}}}{k_{\mathrm{ET}} + k_{\mathrm{PT}}}. \quad 1.$$

The overall reaction is thus described by conventional treatments of ET (11) and PT (12). The distinction between stepwise (edge) versus PCET (inside) may become difficult to distinguish if the second step is fast, i.e., the intermediate state cannot be observed.

Conversely, an authentic PCET reaction has no intermediate. The different pathways within the parallelogram are of significant consequence to the overall rate of the reaction. Within the context of Figure 1, PCET along a strict diagonal path accounts for electron and proton transfer that occurs with minimal charge buildup in the transition state. Other PCET trajectories may require some degree of initial polarization along either the electron or proton coordinate to connect the initial and final states. For paths within the parallelogram

scheme, the degree of collective solvent motion required for the ET versus PT may dictate that one solvent coordinate (ET or PT) is much more likely to dominate the transition state. The height of the barrier and position of the transition state along the reaction coordinate depend on the nature of the pathway. Thermodynamic parameters such as pK_as or reduction potentials may drive the charge to separate via a more PT-like or ET-like transition state as long as the medium can support the increased polarization. It is important to reiterate that all paths within the square are described by a single transition state and may be thought of as concerted despite the polarization of the transition state.

Conflicting nomenclature has been used to describe the various pathways in PCET, and this nomenclature is a source of confusion to the uninitiated. Scheme 1 presents a summary of the various nomenclatures used by prominent authors in this field. General agreement has been reached for the stepwise reactions, ETPT or PTET. Descriptions of pathways within the square are more ambiguous. Acronyms of CEP, CPET, and EPT account for a concerted PCET. However, such formalisms are not entirely satisfying in that they do not describe the degree of charge polarization (i.e., distance from the diagonal) that may be encountered at the transition state. Additional distinctions must be made depending on the nature of the proton acceptor. Transfer of the electron and the proton to the same acceptor has been classified as unidirectional PCET, and bidirectional PCET describes reactions with separate PT and ET acceptors. Varied nomenclature has arisen around the directionality of PCET, such as multisite electron-proton transfer designation (4), which is synonymous with bidirectional PCET.

PCET is intrinsically a quantum mechanical effect because both the electron and proton tunnel, owing to overlap between the donor and acceptor wavefunctions (13). The proton rest mass is ~2000 times that of the electron, and as such, the proton wavelength is ~40 times shorter than that of an electron at a fixed energy. Consequently, PT is fundamentally limited to short distances, whereas the electron, as the lighter particle, may transfer over very long distances (14, 15). Enzymes have evolved to manage these disparate length scales for transfer of the proton and electron. When the electron and proton are required to transfer together, as in activation of substrates via hydrogen atom transfer, the transfer distances are kept short by docking of the substrate within hydrogen bond contact of the enzyme active site. For the purposes of long-distance transport of redox equivalents, the electron and proton need not transfer together, and consequently, the ET and PT coordinates may be orthogonalized by the enzyme in a bidirectional PCET. In this case, PT is confined within a hydrogen bond, whereas ET may occur over many angstroms between separated electron D–A pairs. Adding to the challenge of effecting PCET over long distances with appreciable rates are the requirements that charge transport occur under physiological conditions, with minimal thermodynamic driving force, with low overpotentials, and with specificity.

This review seeks to reveal fundamental aspects of PCET by examining three case studies for which there are strong parallels between molecular model systems and natural biological systems. Our treatment begins with a brief introduction to PCET theory and to the parameters that define and control it. We then focus on three areas of mechanistic enzymology in which PCET is essential to function: electron tunneling through hydrogen

bonds, substrate activation at metallocofactors, and amino acid radical generation and transport.

THEORETICAL TREATMENTS OF PROTON-COUPLED ELECTRON TRANSFER

Marcus' treatment of ET provides a contextual starting point for the PCET reaction (16–18). Analysis of the nonequilibrium free-energy changes associated with electron localization on the donor and acceptor led to the Marcus expression,

$$k_{\mathrm{ET}} = k_{\mathrm{ET}}(0)\exp\left[\frac{-(\lambda+\Delta G^{\circ})^2}{4\lambda \mathrm{R}T}\right], \quad 2.$$

where ΔG° is the driving force for the reaction, λ is the energy needed to reorganize the nuclear configuration of the system from the equilibrium configuration of the reactant state to the transition state, and k_{ET} (0) is the activationless ($\Delta G^{\circ} = -\lambda$) ET rate constant. Marcus succinctly formulated the reorganization energy, λ, as the sum of energies required to reorganize the bond lengths and angles of the redox cofactor (the inner sphere reorganization energy, λ_i) and the surrounding medium (outer sphere reorganization energy, λ_o). The Franck-Condon principle states that nuclear distances and velocities do not change during an electronic transition. In the case of an ET reaction, the electronic transition occurs from the reactant-to-product surfaces. The Franck-Condon principle, therefore, confines ET to occur at a constant nuclear configuration and energy. In classical treatments of ET, such as Marcus theory, the Franck-Condon condition is uniquely satisfied at the intersection of the reactant and product surfaces (at Q^* in Figure 2) (16). As represented at the top of Figure 2, the nuclear configuration of the transition state optimally supports the instantaneous tunneling of an electron. In the original Marcus formulation, the electron tunnels every time the transition state configuration is attained (i.e., the reaction is said to be adiabatic). Subsequent theory refined this assumption by incorporating the quantum mechanical effect of electronic coupling. In Figure 2, the electronic coupling is accounted for by H_{AD}. The reactant and product diabatic surfaces split near the intersection, often referred to as the "avoided crossing," with the magnitude of the splitting equal to twice the electronic coupling. For an adiabatic ET reaction, $2H_{\mathrm{AD}}$ is large, significantly decreasing the activation energy, and ET occurs nearly every time the reactants reach the transition state. For the nonadiabatic case, the electronic coupling is small, and the reactants cross the transition state many times before the electron is transferred to the product energy well. The distance dependency of the electronic coupling term is often accounted by

$$H_{\mathrm{AD}} = H^{\circ}_{\mathrm{AD}}\exp[\beta(r_{\mathrm{AD}} - r_{\mathrm{o}}) \quad 3.$$

where r_o is the center-to-center distance of the D–A pair at contact and β is a constant (19), reflecting the alacrity at which the exponential wavefunction decays. Modification of Equation 2 to include electronic coupling yields the Marcus-Levich-Hush equation for ET (16, 20–22):

$$k_{ET} = \frac{H_{AD}^2}{\hbar}\left(\frac{\pi}{\lambda RT}\right)^{1/2} \exp\left[\frac{-(\Delta G^\circ + \lambda)^2}{4\lambda RT}\right], \quad 4.$$

In a PCET reaction, every parameter is affected by the proton. As the electron moves, the pK_as of redox cofactors change, but to predict the kinetics, knowledge of the driving force of the reaction alone is insufficient. The charge redistribution resulting from electron and proton motion will affect the energy associated with the reorganization of the surrounding environment. In addition, the electronic coupling depends on overlap of both the electronic and proton vibrational wavefunctions of the donor and acceptor states, each of which will change parametrically with the proton coordinate. It should be emphasized that any motion of the proton from its initial position will perturb H_{AD}, ΔG°, and λ; consequently, complete transfer of the proton is not required for PCET to be manifest. At a more extreme level, PCET falls outside the confines of conventional theory because the process includes the breaking and making of chemical bonds. Hence, the applicability of the Born-Oppenheimer and Condon approximations on which most theory is based is somewhat tenuous (2, 23–25).

The PCET problem steps beyond ET because both the electron and the proton affect H_{AD} and the Franck-Condon (FC) term in Equation 4. As mentioned in regard to Figure 2, the electron tunnels through the potential barrier from D to A when the medium fluctuates to a configuration where the energies of the electron donor and acceptor are equal at the surface crossing. For a PCET reaction, the problem is intrinsically more complicated because both the electron and proton tunnel. These tunneling events are also induced by fluctuations in the medium, but now the electron and proton influence each other thermodynamically and kinetically. As the electron moves, the pK_a of the oxidized cofactor will change; but to predict kinetics, the driving force of the reaction is not sufficient. The FC factors will be affected by the charge redistribution resulting from electron and proton motion. In addition, the electronic coupling will change parametrically with the proton coordinate. It should be emphasized that any motion of the proton from its initial position will perturb H_{AD} and the FC terms (ΔG° and λ) and, consequently, the PCET kinetics; complete transfer of the proton is not required.

The original theoretical treatment of PCET by Cukier incorporated the proton into the ET picture by adding a second dimension (9) as shown in Figure 3. Here the reactants and products are described by parabolic potential energy surfaces, which are functions of the solvent response to changes in both the electron (z_e) and the proton (z_p) positions (26). Hammes-Schiffer expanded PCET theory by deriving a kinetic expression in the limit of electronically adiabatic PT and electronically nonadiabatic ET (24):

$$k = \frac{2\pi}{\hbar}\sum_{\mu} P_{I_\mu} \sum_{v} V_{\mu v}^2 (4\pi\lambda_{\mu v} k_B T)^{-1/2} \times \exp\left[\frac{-(\Delta G_{\mu v}^\circ + \lambda_{\mu v})^2}{4\lambda_{\mu v} k_B T}\right], \quad 5.$$

where $\sum_\mu$ and $\sum_\nu$ indicate a sum over vibrational states associated with ET states I and II, respectively, and P_{I_μ} is the Boltzmann factor for state I_μ. In this formalism, each vibrational mode or channel in the reactant well couples to the product well with a different electronic

coupling, $V_{\mu\nu}$, and the overall rate for each vibrational mode is weighted by the Boltzmann factor for thermal population of that channel. Thus, at extremely low temperatures or for high-energy vibrations, only the ground state reactant vibrational mode is populated and contributes to the rate. With knowledge of the experimental rate constant and overall reaction driving force, the reorganization energies, electronic couplings, and percent contribution to the rate for each reactant-product vibrational channel can be computed theoretically. Although not predictive a priori, this theory provides a framework in which PCET reactions may be insightfully analyzed (26).

Savéant and coworkers have recently simplified this formalism to study PCET oxidation of hydrogen-bonded phenols with the following expression (27):

$$k = Z\exp\left[\frac{-\lambda}{4RT}\left(1+\frac{\Delta G^{\circ}}{\lambda}\right)^{2} - \frac{\Delta \mathrm{ZPE}}{RT}\right], \quad 6.$$

where Z is related to the probability of proton tunneling and ET. ΔZPE (= $ZPE^{\ddagger} - ZPE_{R}$) is the change in zero-point energy of the proton vibration at the transition state as compared to the reactant state. ΔZPE can be estimated from the deuterium isotope effect for an adiabatic reaction depicted in Figure 4. A Born-Oppenheimer approximation is used to separate the transferring proton vibrational wavefunction from that of the rest of the nuclear coordinates. The colored circles represent the vibrational energy wavefunction for the transferring proton. Maximal overlap between the proton vibrational wavefunction occurs at the transition state of the PCET reaction. A second Born-Oppenheimer approximation is used at the transition state, such that the electron crosses the barrier while the proton tunnels via vibrational wavefunction overlap. Equation 6 assumes that PCET occurs with the transferring proton at the vibrational ground state in the reactant and product energy well. Adiabatic reactions are predicted to exhibit small isotope effects.

Equation 6 assumes that the proton vibrational wavefunction overlap is static on the timescale of PCET. However, thermal fluctuations can perturb the PT distance on the timescale of PCET. Klinman and coworkers (28–30) have invoked Kuznetsov & Ulstrup's (31) formalism to examine hydrogen tunneling reactions of C–H activation in enzymes with fluctuating hydrogen transfer distances. Equation 7 separates the rate of the hydrogen atom transfer (HAT) into three components: an electronic coupling term (V_{el}), a Marcus-type term describing the barrier for HAT, and a FC gating term, which accounts for the dynamic fluctuation of the hydrogen transfer distance and its effect on the probability of proton tunneling.

$$k = \frac{|V_{el}|^{2}}{\hbar}\left(\frac{\pi}{\lambda RT}\right)^{1/2} \times \exp\left[\frac{-(\Delta G^{\circ}+\lambda)^{2}}{4\lambda RT}\right] (\mathrm{FC\ \ term})^{\mathrm{gating}} \quad 7.$$

In Equation 8, m_H, ω_H, r_H are the mass, frequency, and distance traveled by the transferring proton, $X = r_X\sqrt{m_X\omega_X/\hbar}$, and m_X, ω_X, r_X represent the mass, frequency and distance traversed by the fluctuating barrier. This formalism assumes nonadiabatic PT and ET. The magnitude of the KIE is determined by the FC term and is proportional to the D–A distance.

A similar result is obtained within the context of Equation 5 (32). The temperature dependency of Equation 7 arises from the Marcus expression and the FC term. The *T* dependency of the Marcus term should be independent of isotope as long as HAT occurs from the lowest energy vibration, whereas the *T* dependency of the FC term should dramatically depend on the isotope. Thus, the temperature dependency of the KIE can be a powerful experimental probe of the elements of Equation 7 that dominate the reaction barrier. A KIE that is highly *T* dependent suggests a large degree of distance sampling at the transition state (*vide infra*).

$$(\mathrm{FC\ \ term})^{\mathrm{gating}} = \int_{r_1}^{r_0} \exp\left[\frac{-m_H \omega_H r_H^2}{2\hbar}\right] \times \exp\left[\frac{-\hbar\omega_x X^2}{2RT}\right] dX \quad 8.$$

ELECTRON TRANSFER THROUGH HYDROGEN BONDS

PCET emerged as a field of study at a mechanistic level with the examination of electron transfer from a donor (D) to an acceptor (A) juxtaposed by a hydrogen-bonding interface (—[H$^+$]—). In D—[H$^+$]—A, the electron must contend with the proton in its journey from D to A. It is important to emphasize that the proton does not have to be formally transferred within the interface for a PCET effect to be observed. All that is required for a PCET event is that the kinetics (and thermodynamics) of electron transport depends on the position of a specific proton or set of protons at any given time. Furthermore, the same electron and proton do not have to be coupled throughout an entire process. As the electron moves, it may encounter different protons along a transport chain. To this end, the long-distance transfer of electrons in biology will often exhibit the characteristics of PCET.

Metallolabeled Proteins

Long-distance ET in proteins involves electron tunneling through a heterogeneous polypeptide environment (14, 15). Gray and coworkers (15, 33, 34) have measured the ET tunneling rates between Ru^{II} complexes labeled at surface His residues and the metallocofactors of Zn-cyt *c*, myoglobin (Mb), high-potential ironsulfur protein (HiPIP), azurin, plastocyanin, stellacyanin, cyt b_5, and cyt c_{55} (15). Figure *5a* illustrates this labeling strategy with the X-ray crystal structure of oxidized azurin(Cu^{2+}) appended with a Ru(tpy)(phen)(His83)$^{2+}$ label (35). To determine a reliable value for the electronic coupling, H_{AD} in Equation 4, on the overall reaction rate, the temperature dependency of the reaction driving force, and rate constant must be measured to ensure that the reactions are activationless (with $-\Delta G^\circ \approx \lambda$). By labeling the protein at different sites, the distance dependency on the overall ET rate may be used to estimate the electronic coupling (β in Equation 3).

Theoretical models (36, 37) have been developed to dissect the electron tunneling pathways in proteins. A particular challenge is the requirement that the structural complexity of the protein matrix, especially the array of bonded and nonbonded contacts, be properly accommodated. In the tunneling-pathway model, the medium between metallocofactor and appended metal center is decomposed into smaller subunits linked by through-bond, through-space, and hydrogen-bond-mediated interactions, ε_C, ε_S, and ε_H, respectively (38):

$$H_{AD} \propto \prod \varepsilon_C \prod \varepsilon_S \prod \varepsilon_H \quad 9.$$

with the coupling decay constant for a hydrogen bond defined as

$$\varepsilon_H = \varepsilon_C^2 \exp[-1.7(R - 2.8). \quad 10.$$

The coupling decay through a hydrogen bond is therefore thought of as the coupling through two covalent bonds (with $\varepsilon_C = 0.6$) with an added distance dependency if the bond length is longer or shorter than the reference value (2.8 Å for two bonds) (38).

From these experimental and theoretical studies, a generalized picture for ET through hydrogen bonds in proteins and enzymes has emerged. Judicious placement of ET probes about the protein surface has shown that secondary structure has a profound effect, and hydrogen bonds of α-helices and β-sheets play a critical role. Some data suggest that β-sheets appear to mediate coupling more efficiently than do α-helices (theoretical β(α-helix) ~1.4 $Å^{-1}$ β(β-sheet) ~1.1 $Å^{-1}$) (39, 40). The established hydrogen bond interactions within the folded protein, however, will determine whether α-helices are better than β-sheets in mediating long-range electronic coupling for a given protein (17). Whereas ET in proteins has provided a holistic picture of electron tunneling through hydrogen bonds in proteins, hydrogen-bonded supramolecular assemblies have proven to be incisive in advancing an understanding of how the proton precisely couples to the electron as it tunnels through a hydrogen bond.

Hydrogen-Bonded Electron Transfer Donor-Acceptor Dyads

Isolation of the ET pathway to a single hydrogen bond has revealed that charge transport is indeed a PCET (as opposed to simple ET tunneling) event. Detailed studies have been performed on ET D–A supramolecules assembled through a hydrogen-bonded interface (—[H^+]—) (8). One such D—[H^+]—A construct (with [H^+] = [$(COOH)_2$], D = zinc(II) porphyrin, A = dinitrobenzene, **1** in Figure *5b*) exploited the propensity of carboxylic acids to form cyclic dimers in low-polarity, nonhydrogen-bonding solvents (41). Observation of a deuterium isotope effect for charge separation and recombination revealed the coupling between electron and proton. Within the [$(COOH)_2$] interface, proton displacement on one side of the dicarboxylic acid interface is compensated by the concomitant displacement of a proton from the other side. Because charge redistribution within this interface is negligible, the only available mechanism for PCET arises from the dependency of the electronic coupling matrix element on the position of the protons within the interface (9, 42, 43). As the proton configuration changes, so does the electronic matrix element, and, consequently, the ET rate depends on the proton configuration and dynamics. Similar results have been obtained for donors and acceptors separated by guanine-cytosine base pairs (44–46) and related interfaces (8, 47) where net proton motion within the interface is minimal.

Polarized hydrogen bonds within an interface may be constituted from asymmetric interfaces between D–A pairs (48–52). A prominent archetype used for PCET studies is the amidinium-carboxylate salt bridge, which approximates the important structural element in

biology—the arginine-aspartate (Arg-Asp) salt bridge. But unlike Arg-Asp, which has multiple guanidinium-carboxylate interactions, the amidinium presents only two N–H bonds for hydrogen bonding to carboxylate (Scheme 2), thereby simplifying PCET studies.

The pronounced effect of the proton on the ET rate is immediately evident from a comparative kinetics study of a D— [amidinium-carboxylate]—A complex and its inverted interfacial D—[carboxylate-amidinium]—A counterpart (D = $Ru(bpy)_3^{2+}$, A = dinitrobenzene, **2** in Figure *5b*) (48, 50). The rate of charge transfer between donor and acceptor along a linear D– (carboxylate-amidinium)–A pathway ($k_{PCET} = 3.1 \times 10^8\ s^{-1}$) is attenuated ~40-fold when the interface is switched, D–(amidinium-carboxylate)–A. From these experiments, we find that the driving force and reorganization energy depend on the charge distribution of the electron and the proton because the initial and final charge values are dependent on whether the process corresponds to ET, PT or PCET. Therefore, the two parameters that determine the rate of a charge transfer reaction, the activation energy and the electronic coupling, depend on the reaction pathway (53). The coupling of the charge shift resulting from electron and proton motion to the polarization of the surrounding environment thus embodies the essential distinguishing characteristic of a PCET reaction.

The effects of tunneling on PCET rates through salt bridges have been uncovered with assembly **3** shown in Figure *5b*. Photoexcitation of the Zn(II) porphyrin photoreductant prompts ET to the naphthalene diimide electron acceptor via the amidine-carboxylic acid hydrogen-bonded bridge (54, 55). This reaction may be followed by monitoring the growth and decay of the porphyrin cation radical transient absorption ($k_{PCET}(fwd) = 9 \times 10^8\ s^{-1}$ and $k_{PCET}(rev) = 14 \times 10^8\ s^{-1}$). The nuclear and electronic contributions to the PCET reaction may be unraveled from temperature-dependent kinetics measurements (56). A small electronic coupling term ($V = 2.4\ cm^{-1}$) supports the contention that the hydrogen-bonding interface is the bottleneck for electronic coupling in this system. Extending the temperature-dependent measurements to a deuterated bridge yields a KIE that switches from being normal at high temperature (k_H/k_D ~1.2, 300 K) to inverted at low temperature (k_H/k_D ~0.9, 120 K) (Figure *6a*). This is interpreted in a model where fluctuations within the hydrogen-bonding bridge dynamically modulate electronic coupling for ET, and consequently, the rate of charge separation becomes sensitive to the nature of proton modes within the bridge (25). Thermal population of vibrational states is the most likely cause of the reverse isotope effect in this system, where the low-frequency mode is a localized 3-atom N–H—O vibration in the hydrogen bond. The energy between the ground and excited vibrational modes ($\hbar\omega$) (Figure *6b*) is larger for the proton compared to the deuteron. At low enough temperatures, a situation may result such that the excited-state vibrational modes of the deuterated salt bridge may be thermally accessed while the protonated bridge remains in the vibrational ground state ($v = 0$) mode. Excited-state vibrational wavefunction overlap (red section in Figure 6) facilitates electron tunneling from the reactant to the product well. Thus at low temperatures, the population of the excited-state mode for the deuterated salt bridge increases the rate of ET, whereas the protonated salt bridge must rely on more sluggish tunneling from the $v = 0$ mode, resulting in the inverse isotope effect. The normal isotope effect is recovered with increasing temperature as the lowest lying excited states of the hydrogen bond vibration of interest begin contributing to the PCET rate. The unusual

isotope behavior has also been observed for the oxidation of a model ubiquinol (UQH_2-0) cofactor by the photoactive ruthenium complex **4** (Figure *5b*), $Ru(bpy)_2(pbim)^+$(bpy=2,2′-bipyridine;pbim= 2-(2-pyridyl)benzimidazolate), which mimics the PCET reactivity and hydrogen-bonding ability of the Rieske [2Fe2S] center in the cytochrome b_{c1} complex (57). A KIE that switches from being normal at high temperature to inverted at low temperature suggests that the oxidation of the ubiquinol in the model complex (and most likely the biological) system proceeds via unidirectional PCET in which the UQH_2-0 substrate is hydrogen bonded to the redox cofactor. As described for model system **4** of Figure *5b*, this behavior is indicative of PCET through the hydrogen bond as the bottleneck for charge transport.

ACTIVATION OF SUBSTRATE C-H BONDS

The removal a hydrogen atom, H atom, $H^{\bullet}$, from a substrate requires the transfer of an electron and proton. To this end, the HAT reaction is a subclass of PCET. HAT is defined as the transfer of an electron and a proton from one location to another along a spatially coincidental pathway. In a traditional radical HAT abstraction, the electron comes from the X–H bond (typically sigma), and transfers co-linearly with the proton to become part of the new H–Y bond. In this case, the electron and proton are donated from one atom, and they are accepted by another atom. These transfers are well described mechanistically as the diagonal pathway of Figure 1. However, many reactions treated within a formalism of HAT are more complex as ET and PT are site differentiated either along uni- or bidirectional pathways. This is the case for lipoxygenase and the Fe^{III} complexes that model the PCET reactivity of the enzyme.

Hydrogen Tunneling in Enzymes

Enzymatic activation of C–H bonds occurs by PCET as the overall process entails the abstraction of an electron and proton from the substrate (58–61). Owing to the sensitivity of proton tunneling on distance, PCET provides a mechanism by which enzymes may derive substrate selectivity. This contention is supported by Klinman and coworkers' KIE measurements (58) of the oxidation of benzyl alcohol to benzaldehyde by yeast alcohol dehydrogenase (YADH). Hydrogen atom tunneling is revealed by primary and secondary protium-to-tritium (H/T) and deuterium-to-tritium (D/T) KIE. Hydride transfer from the alcohol to the oxidized nicotinamide adenine dinucleotide co-factor of YADH is rate limiting, and thus, the measured catalytic rate is a direct probe of the chemistry at the active site. In the absence of tunneling, the transfer rate of different isotopes of hydrogen may be assumed to vary owing to the difference in zero-point vibrational energy of the C–(H/D/T) bond. The rate of hydrogen, deuterium, and tritium tunneling (k_H, $k_{D,}$, and k_T, respectively) may then be interrelated by the reduced mass of the C–(H/D/T) bond (62, 63):

$$(k_H/k_D)^{1.44}=k_H/k_T. \quad 11.$$

$$(k_D/k_T)^{3.26}=k_H/k_T. \quad 12.$$

These relationships hold for both the primary (transferring H) and secondary (stationary H) isotope effects. Of the three isotopes, protium is the most likely to tunnel owing to its lighter mass and longer wavelength. Inflated experimental values of the exponents are indicative of faster hydrogen transfer than classically predicted and thus provide a metric for the tunneling contribution to the overall reaction. Larger primary (3.58 ± 0.09) and secondary (10.2 ± 2.4) exponents (58) are observed for the oxidation of benzyl alcohol by YADH with tritium as the common atom (Equation 12). This work provided some of the first unequivocal evidence for tunneling in the C–H activation reactions of enzymes.

More compelling evidence for hydrogen tunneling has been observed for the C–H activation of linoleic acid (LA) (Figure 7*a*) by soybean lipoxygenase-1 (SLO-1) (64, 65). In this system, a Fe^{3+}-OH cofactor abstracts an $H^{\bullet}$ from the C-11 carbon atom of the physiological LA substrate. The PCET nature of the reaction is revealed by a weak temperature dependency (E_{act} = 2.2 kcal/mol), a small Arrhenius prefactor ($A_H < 10^5\ s^{-1}$) and a large deuterium KIE on k_{cat} (k_H/k_D = 81) (66), all of which are experimental markers for a proton tunneling event that accompanies ET. Striking reactivity was observed with site-directed mutants of SLO (*L754A*, *L546A*, and *I553A*) that open the binding pocket of the substrate in the enzyme active site (28). Although the *I553A* mutant exhibits k_{cat} and E_{act} values similar to that of wild-type SLO, the KIE becomes highly temperature dependent. Evaluated within the context of Equation 7, the temperature-dependent isotope effect data reveal dynamic fluctuation of the hydrogen transfer distance that affects the probability of hydrogen tunneling. This result suggests that a loosening of the binding pocket induces significant distance sampling (i.e., gating) of the $H^{\bullet}$ abstraction reaction (28). KIE data analyzed within a PCET formalism that includes the explicit environment of the enzyme active site (32) supports this contention. Together, these data suggest that the structure of the wild-type SLO enzyme has evolved to minimize this distance sampling and facilitate facile C–H activation (28). To this end, PCET brings a new perspective to the “lock-and-key” (67) and “induced-fit” (68) models of enzyme active sites. Whereas similar substrates may sample an enzyme active site in a PCET reaction, rates of substrate activation may be significantly attenuated with respect to k_{off} if the PT tunneling distance is not optimized for PCET. Owing to the considerable sensitivity of proton tunneling to distance, PCET provides biology with an exquisite mechanism for achieving substrate selectivity.

PCET in a Lipoxygenase Model Complex

Do the electron and proton transfer as a hydrogen atom in the initial C–H activation step of SLO? This question has been addressed with the model system of a deprotonated Fe(*tris*-bi-imidazoline)$^{2+}$ [Fe^{III}(Hbim)] complex and dihydroanthracene (69, 70). The overall C–H activation reaction is depicted in Figure *7b*. The electron and proton are transferred from the C–H bond of DHA to different orbitals on the metal complex: the electron to a metal-based *d*-orbital and the proton to a N-based lone pair orbital on the Hbim ligand. Ther-modynamic analysis of the individual reagents suggests that the stepwise ET and PT pathways are significantly endergonic, whereas CEP is uphill by only ~2 kcal mol^{-1}. Consequently CEP is favored over initial ET or PT by 53 and 30 kcal mol^{-1}, respectively. Analysis of the temperature dependency of the second-order rate constant affords a barrier for the C–H activation of $\Delta G^{\ddagger}$ = 22 kcal mol^{-1}. Thus, the observed barrier is smaller than the calculated

driving force for either initial ET or PT, suggesting that the C–H activation of DHA by Fe^{III}(Hbim) proceeds via the CEP mechanism, rather than a HAT. This reactivity parallels the SLO system in which the electron and proton from the C–H bond are transferred to discrete and different sites of the SLO cofactor—the proton is transferred to the lone pair on the hydroxide ligand and the electron is transferred to a *d*-orbital on the Fe^{3+} metal.

As highlighted by SLO and model complex reactivity, C–H radical abstraction by metallocofactors differs from the traditional definition of a HAT reaction. In a traditional HAT, the electron originates from the X–H bond (typically sigma) and transfers colinearly with the proton to become part of the new H–Y bond. From the perspective of PCET, the close-range linear orbital pathway makes it reasonable that the electron and proton transfer adiabatically in a synchronous manner along the diagonal of Figure 2. In the H–abstraction mechanisms of metallocofactors, although the electron and proton originate from the same bond of the substrate, the electron and proton are often site differentiated at the cofactor. Considerable charge separation may accompany the reaction by virtue of the site differentiation of the electron and proton. Hence, PCET, as opposed to classical HAT, is a more complete and accurate description of the overall enzyme kinetics of C–H reactivity at metallocofactors (71).

PROTON-COUPLED ELECTRON TRANSFER OF AMINO ACID RADICALS

Amino acid radicals are commonly used as redox-active cofactors and charge transport intermediates in enzymes (72–74), and the PCET mechanisms of their generation and reactivity are currently an active area of research (3, 75– 77). Oxidation of amino acids at physiological pH usually involves the loss of both a proton and electron, implicating PCET as the redox mechanism. Free amino acid radicals in solution typically have a micro- to millisecond lifetime, yet nature has evolved enzymes to manage both the proton and electron equivalents in harnessing the oxidative power of these intermediates for chemical transformations. Of the many enzymes that operate by mechanisms involving radicals (74), the most detailed PCET analysis of radical generation and transport have been performed on photosystem II (PSII) and ribonucleotide reductase (RNR). As discussed below, the kinetics of tyrsoine radical generation may be isolated in model systems in which tyrosine radical production is turned on instantaneously with the production of the excited state of a metal complex covalently attached to tyrosine.

Photosystem II

PSII harvests light to generate a charge-separated state that is a weak reductant but a powerful oxidant capable of oxidizing H_2O to O_2 (78). Light drives ET along a chlorophyll *a* (P680), pheophytin *a*, and quinone (Q_A and Q_B) network (79). The conversion of light energy to chemical energy occurs by the double reduction of Q_B to quinol (Q_BH_2), which is at the terminus of an ET network. The Q_BH_2 diffuses into the membrane toward the cytochrome b_6f complex, where it is oxidized to release protons across the membrane into the periplasm, generating a proton gradient that drives ATP synthesis. Although the generation of Q_BH_2 has yet to be examined in PSII, the generation of the two-electron/proton carrier has been shown to occur by multiple PCET steps in the bacterial reaction center (80). In the first light-induced reaction, one-electron reduction of Q_B by Q_A^- is

coupled to the protonation of a nearby Glu-L212. A second light-induced ET from Q_A^- is driven by protonation of Q_B^-. This latter reaction was shown to proceed by a two-step process in which fast protonation precedes the rate-limiting ET.

The electron-hole equivalent that is left behind on the oxidized $P680^+$ is ultimately transferred to the $CaMn_4$ oxygen-evolving complex (OEC) of PSII, which is responsible for water oxidation. Four flashes of light are required for O_2 evolution, and each flash steps the OEC through a different redox state, S_0 through S_4, with the S_4 to S_0 transition occurring in the dark with thermal release of O_2 (81–84). The donor to $P680^+$ was identified by Babcock and coworkers (85) as a tyrosyl radical, which was later identified as Y161 (Y_Z) of the D1 polypep-tide (86, 87). Site-directed mutagenesis studies revealed that the presence of H190 facilitated oxidation of Y_Z by $P680^+$ by a factor of at least 200, implicating hydrogen bonding between these residues and indicating the importance of this hydrogen bond in facilitating Y_Z oxidation (88–90). PCET was identified as the mechanism for Y_Z oxidation with ET to $P680^+$ and PT to H190 (91, 92). The results of a recent crystal structure of PSII (93) presented in Figure *8a* clearly support the existence of hydrogen bonding between Y_Z and H190 and an ET tunneling pathway comprising $P680 \rightarrow Y_Z \rightarrow OEC$ (Mn_4Ca). These results show PSII to be an exemplar of bidirectional PCET. The electron, as the lighter particle, can tunnel over much longer distances between the redox-active cofactors, whereas proton tunneling is restricted to the short distance provided by the hydrogen bond between H190 and Y_Z.

Ribonucleotide Reductase

Class I *Escherichia coli* ribonucleotide reductase (RNR) plays a crucial role in DNA replication and repair by catalyzing the reduction of nucleoside diphosphates (NDPs) to deoxynu-cleoside diphosphates (dNDPs) (94, 95). The enzyme is composed of two homodimeric sub-units designated α2 and β2, and a complex between the two is required for activity (96). α2 houses the NDP-binding sites and the binding sites for the effectors that control the specificity and rate of nucleotide reduction (96–98). β2 harbors a diferric tyrosyl radical (•Y122) cofactor proposed to initiate nucleotide reduction by oxidizing a cysteine residue (C439) in the active site of α2 (99).

The crystal structures of both subunits have been solved independently (100–102), and a docking model of the two proteins in a 1:1 complex has been generated on the basis of their complementary shapes and on knowledge of conserved residues (100). In this model, more than 35 Å separate the •Y122 on β2 from C439 in α2; this long distance has recently been verified by PELDOR studies of the mechanistically inhibited α2:β2 complex (103). Superexchange electron tunneling between •Y122 and C439 based on Marcus theory ($k_{ET} = 10^{-6}\ s^{-1}$ for $\beta = 1.2\ Å^{-1}$ under activationless conditions) is too slow to account for a k_{cat} of ~2 to 10 s^{-1} (16). Thus, the radical generation process has been proposed to occur via a hopping mechanism involving conserved amino acid residues •Y122→W48→Y356→Y731→Y730→C439 as shown in Figure 8 (75, 100). Site-directed mutagenesis studies confirm that these residues are required for activity (104–107), although they do not provide additional information regarding the precise mechanism of radical transport.

Presteady-state stopped-flow experiments have been performed to probe the mechanism of radical transport in *E. coli* RNR. No changes in the •Y122 concentration could be detected upon mixing the α2 and β2 subunits under a variety of conditions. These data supported a model in which a rate-limiting physical or conformational step was required in the α2:β2 complex for radical transport and subsequent active site chemistry to occur (108). Using intein protein ligation methods, semisynthetic β2 subunits were generated with unnatural amino acids at position 356 (109–112). In particular, a series of fluorinated tyrosine derivatives were generated with reduction potentials that varied from −50 mV to +270 mV relative to tyrosine over the accessible pH range for RNR and pK_as that ranged from 5.6 to 9.9 (113). The pH rate profiles of deoxynucleotide production by these F_nY356-β2s were reported, and the results suggested that the rate-determining step in RNR activity could be changed from the physical step to the radical propagation step, by altering the reduction potential of •Y356 with these analogs (112). These studies supported the model that Y356 is a redox-active amino acid on the radical propagation pathway. Furthermore, several of the F_nY356-β2s are deprotonated at pH > 7.5 and efficiently initiated nucleotide reduction. Thus, a proton is not obligated to the pathway between W48 and Y356 of β2 and Y731 of α2, nor is HAT between these residues obligatory for radical propagation.

The Y731↔Y730↔C439 triad in the α2 subunit connects Y356 of β2 to the active site via a hydrogen bond network. As shown in Figure *8a*, the triad is in hydrogen-bonding contact. The in vivo suppressor tRNA/aminoacyl-tRNA synthetase method (114) has recently been employed to site specifically incorporate 3-aminotyrosine (NH_2Y) at positions 731 and 730 (115). The reduction potential of $NH_2Y^•$ is 0.19 V lower than that of Y•, therefore NH_2Y730/731 serves as an effective thermodynamic trap in radical transport. Upon mixing NH_2Y730/731α2 with β2 in the presence of RNR substrate and effector, followed by freeze-quenching of the reaction, a new organic radical was observed in the X-band electron paramagnetic resonance spectrum that was attributed to $NH_2Y730/731^•$ (115). Surprisingly, the mutants retained activity, albeit at levels attenuated from that of wild type. These experiments provide direct evidence that Y730 and Y731 are redox-active residues in the radical transport pathway of RNR, although they do not report on the PCET mechanism for radical formation.

To study PCET in α2, we have constructed photoRNRs (116). The 20-mer C-terminal peptide tail (β2C20, NH_2– YLVGQIDSEVDTDDLSNFQL–COOH) of the β2 subunit contains the critical Y356 and the binding determinant of β2 to α2 (117, 118). Using solid-phase peptide synthesis, the C-terminal peptide tail of β2 is produced with a photo-oxidant appended proximal to Y356 on the peptide. Laser excitation of the modified peptide provides a method to generate •Y356, therein bypassing hole generation at the metallocofactor and allowing the PCET pathway in α2 to be “turned on.” Single turnover experiments with the peptide bound to α2 and in the presence of CDP substrate and ATP effector establish that the enzyme is active when excited by light and inactive in the absence of excitation (119–121). Mutation of Y730 to F breaks the hydrogen bond network in α2 and increases the electron and proton tunneling distance, as now the radical must tunnel directly from C439 to reduce the hole on $Y731^•$. This mutant is effectively inactive toward

photoinitiated nucleotide reduction. This result provides strong evidence that radical transport is indeed pathway specific in α2 and suggests a colinear PCET pathway.

A model that accounts for PCET in RNR is shown on Figure 8*a*. Beginning at the cofactor, an orthogonal PT between Y122 and the diiron oxo/hydroxo cofactor establishes the need only for the transfer of an electron through the span of β2. Oxidation of Y356, the redox terminus of the β2 pathway, demands a PCET reaction, but this too appears to involve a PT that is orthogonal to the ET pathway. By moving the protons at Y122 and Y356 off pathway, the radical transport in β2 involves a long-distance ET coupled to short PT hops at the tyrosine endpoints. In setting up the radical transport pathway in this fashion, the very different PT and ET length scales are managed in RNR. Within α2, the activity studies of the Ac-(W/BPA)-R2C20 peptide and α2, together with those of the Y730/731F α2 mutant, suggest a colinear PCET pathway through α2 in which both the electron and proton may be transferred among Y731-Y730-C439. Such a transfer is unusual inasmuch as radical transport occurs by committing both the proton and electron to the pathway. In contrast to most systems studied to date in biology, RNR appears to incorporate all the variants of PCET mechanisms in its transport of a radical across two subunits and over 35 Å.

Photoactive Tyrosine Metal Complexes

To more precisely examine the PCET mechanism of the $Y^{\bullet}$ formation, model complexes have been synthesized with Y appended to photo-oxidants $Ru(bpy)_3^{2+}$ (**RuY**) (122), Ru(bpy-4,4′-COOEt)2(bpy)$^{2+}$ (**Ru$_{es}$terY**) (77), or Re(phen)(CO)3(PPh3)$^{+}$ (**Re(P–Y)**) (123) (shown in Figure *8b*). Upon excitation of the complexes with near UV-vis light, Y oxidation is initiated by either of the methods depicted in Scheme 3. Flash quench photochemistry is employed for the **RuY** and **Ru$_{ester}$Y** systems; excitation of the Ru^{II} complex results in a metal-to-ligand charge transfer (MLCT) excited state. The MLCT excited state has a lifetime on the order of hundreds of nanoseconds and can be oxidized bimolecularly by an oxidant in solution (shown in Scheme 3 as methyl viologen, MV^{2+}) to form a Ru^{III} intermediate. The latter is a stronger oxidant than the (triplet) MLCT state and has a lifetime on the order of milliseconds, allowing for oxidation of the appended Y residue, which can be monitored with transient absorption (flash photolysis) spectroscopy (122). **Re(P–Y)** exhibits a longer-lived, more oxidizing MLCT state compared to the Ru^{II} complexes and thus can oxidize the appended Y residue directly, as monitored by quenching of the excited-state emission (123). The measured rate of Y oxidation for all systems can be dependent upon the bulk pH.

A pH dependency in Y oxidation may be explained by a PCET reaction with OH^{-} or basic forms of buffer as the proton acceptor (124, 125). Subsequent experiments confirmed that for **Re(P–Y)**, the strongest oxidant of the series, phosphate buffer in the form of HPO_4^{2-} acts as a proton accepter with the electron transferred from Y to the excited Re* complex and the proton from Y to HPO_4^{2-} (126). This reaction thus mimics the oxidation of the Y_Z-H190 pair in PSII. The pH dependency of the rate was ascribed to titration of the HPO_4^{2-}/$H_2PO_4^{2-}$ equilibrium; accordingly, no pH dependency of the rate of Y oxidation in **Re(P–Y)** was observed in the absence of buffer. Similar effects were also observed with imidazole and pyridine buffers. The Ru^{II}-based systems showed a similar buffer dependency in the rate

of Y oxidation at high (>10 mM) buffer concentrations. However, the rate of Y oxidation in **RuY**, the weakest oxidant in the series, was also shown to increase with pH in the absence of buffer. The complex with intermediate oxidant strength, $\mathbf{Ru_{ester}Y}$, exhibits a pH-independent rate of Y oxidation below pH 7 (no buffer) that becomes pH dependent at high pH (= 10).

Analysis of the charge transfer rates and deuterium isotope effects for each of these systems in the presence and absence of buffer and as a function of pH (pD) revealed the full mechanistic complexity for Y oxidation in this series of compounds (126). For the strong oxidant, **Re(P–Y)**, an ETPT stepwise mechanism for Y oxidation was proposed to occur in the absence of buffer. For the weak oxidant, **RuY**, Y oxidation may proceed via a CEP mechanism with ET to the Ru^{III} intermediate and PT to bulk solution. Both the ETPT and CEP mechanisms may be in competition: The intermediate oxidant, $\mathbf{Ru_{ester}Y}$, was proposed to follow the ETPT mechanism at low pH and switch to the CEP mechanism at high pH. The switching of the mechanisms for $\mathbf{Ru_{ester}Y}$ may be controlled by the pH-dependent reduction potential of $Y^{\bullet}$, which decreases 59 mV/pH unit (127). In the presence of buffer, the reaction was proposed to occur via a CEP mechanism with ET from Y to the oxidant and PT from Y to the basic form of the buffer. Recent theoretical work on the oxidation of Y in **Re(P–Y)** supports such a concerted PCET mechanism with HPO_4^{2-} buffer species acting as the proton acceptor (128).

Similar studies have focused on the oxidation of hydrogen-bonded phenols with appended bases functioning as the intramolecular proton acceptor and with an electrode surface (27, 129) or oxidants in solution (130, 131) as the electron acceptor. In both reports, phenol oxidation occurred via a bidirectional CEP mechanism (ET to oxidant, PT to hydrogen-bonded base). For the homogeneous case, analysis of the temperature dependency of the reaction rate suggested the reactions were adiabatic. Marcus theory analysis led to the conclusion that the CEP reactions of these phenols occur with large reorganization energies, compared to ET reactions for aromatic compounds (131). However, subsequent analysis of the variation in driving force for these reactions with temperature revealed that the homogeneous CEP reactions were, in fact, nonadiabatic and the internal reorganization energies more modest (27). In contrast, the heterogeneous oxidation of the hydrogen-bonded phenol using a glassy carbon electrode proceeds via adiabatic CEP. The variant behavior with choice of oxidant (electrode versus solution oxidant) was postulated to be a result of the strong electric field within which the heterogeneous reaction takes place, which may stabilize the zwitterionic form of the transition state and decrease the proton tunneling barrier (27). Local electric fields within enzymes often enhance reaction rates (132), and it remains to be seen whether such fields influence enzymatic PCET.

ACKNOWLEDGMENT

We acknowledge the stimulating collaboration with Joanne Stubbe on the PCET mechanism of RNR catalysis, as well as all the members of the group, past and present, who have contributed to these fundamental PCET studies over the years. The National Institutes of Health supported this work with grant GM47274.

Glossary

PCET	proton-coupled electron transfer
ET	electron transfer
KIE	kinetic isotope effect
PT	proton transfer
Reorganization energy, λ	the energy associated with nuclear rearrangements, both solvent and internal, required for electron transfer
Electronic coupling (H_{AD})	the energy derived from overlap of the reactant and product electronic wavefunctions
Wavefunction overlap	the magnitude of the integral $\langle \psi' \vert H' \vert \psi \rangle$; ψ' and ψ are initial and final state wavefunctions and H' the coupling Hamiltonian operator
HAT	hydrogen atom transfer
β	the decay constant for the distance dependency of electronic coupling in an electron transfer reaction
SLO	soybean lipoxygenase
PSII	photosystem II
RNR	ribonucleotide reductase
α2	the large subunit of *E. coli* RNR containing the enzyme active site and binding sites for nucleotide activity and specificity effectors
β2	the small subunit of *E. coli* RNR containing the diiron, tyrosyl radical cofactor necessary for catalysis

LITERATURE CITED

1. Reece SY, Hodgkiss JM, Stubbe J, Nocera DG. Proton-coupled electron transfer: The mechanistic underpinning for radical transport and catalysis in biology. Philos. Trans. R. Soc. Lond. Ser. B. 2006; 361:1351–1364. [PubMed: 16873123]
2. Cukier RI, Nocera DG. Proton-coupled electron transfer. Annu. Rev. Phys. Chem. 1998; 49:337–369. [PubMed: 9933908]
3. Mayer JM. Proton-coupled electron transfer: a reaction chemist's view. Annu. Rev. Phys. Chem. 2004; 55:363–390. [PubMed: 15117257]
4. Huynh MHV, Meyer TJ. Proton-coupled electron transfer. Chem. Rev. 2007; 107:5004–5064. [PubMed: 17999556]
5. Pourbaix, M. Atlas of Electrochemical Equilibria in Aqueous Solutions. Oxford: Pergamon; 1966.
6. Westheimer FH. The mechanisms of chromic acid oxidations. Chem. Rev. 1949; 45:419–451.
7. Wiberg KB. The deuterium isotope effect. Chem. Rev. 1955; 55:713–743.
8. Chang, CJ.; Brown, JDK.; Chang, MCY.; Baker, EA.; Nocera, DG. Electron transfer in hydrogen-bonded donor-acceptor supramolecules. In: Balzani, V., editor. Electron Transfer in Chemistry. Weinheim, Ger.: Wiley-VCH; 2001. p. 409-461.

9. Cukier RI. Mechanism for proton-coupled electron-transfer reactions. J. Phys. Chem. 1994; 98:2377–2381.
10. Fang J-Y, Hammes-Schiffer S. Proton-coupled electron transfer reactions in solution: molecular dynamics with quantum transitions for model systems. J. Chem. Phys. 1997; 106:8442–8454.
11. Marcus RA, Sutin N. Electron transfers in chemistry and biology. Biochim. Biophys. Acta. 1985; 811:265–322.
12. Ando K, Hynes JT. Acid-base proton transfer and ion pair formation in solution. Adv. Chem. Phys. 1999; 110:381–430.
13. Hammes-Schiffer S. Hydrogen tunneling and protein motion in enzyme reactions. Acc. Chem. Res. 2006; 39:93–100. [PubMed: 16489728]
14. Moser CC, Keske JM, Warncke K, Farid RS, Dutton PL. Nature of biological electron transfer. Nature. 1992; 355:796–802. [PubMed: 1311417]
15. Gray HB, Winkler JR. Electron transfer in proteins. Annu. Rev. Biochem. 1996; 65:537–561. [PubMed: 8811189]
16. Marcus RA, Sutin N. Electron transfers in chemistry and biology. Biochim. Biophys. Acta. 1985; 811:265–322.
17. Gray HB, Winkler JR. Electron tunneling through proteins. Q. Rev. Biophys. 2003; 36:341–372. [PubMed: 15029828]
18. Moser CC, Page CC, Dutton CC. Darwin at the molecular scale: selection and variance in electron tunnelling proteins including cytochrome *c* oxidase. Philos. Trans. R. Soc. Lond. Ser. B. 2006; 361:1295–1305. [PubMed: 16873117]
19. Hopfield JJ. Electron transfer between biological molecules by thermally activated tunneling. Proc. Natl. Acad. Sci. USA. 1974; 71:3640–3644. [PubMed: 16592178]
20. Levich VG. Present state of the theory of oxidation-reduction in solution (bulk and electrode reactions). Adv. Electrochem. Electrochem. Eng. 1966; 4:249–371.
21. Hush NS. Intervalence-transfer absorption. II. Theoretical considerations and spectroscopic data. Prog. Inorg. Chem. 1967; 8:391–444.
22. Sutin N. Theory of electron transfer reactions: insights and hindsights. Prog. Inorg. Chem. 1983; 30:441–498.
23. Cukier RI. Proton-coupled electron transfer reactions: evaluation of rate constants. J. Phys. Chem. 1996; 100:15428–15443.
24. Soudackov AV, Hammes-Schiffer S. Derivation of rate expressions for nonadiabatic proton-coupled electron transfer reactions in solution. J. Chem. Phys. 2000; 113:2385–2396.
25. Pressé S, Silbey R. Anomalous temperature-isotope dependence in proton-coupled electron transfer. J. Chem. Phys. 2006; 124 164504/1–7.
26. Hammes-Schiffer S. Theoretical perspectives on proton-coupled electron transfer reactions. Acc. Chem. Res. 2001; 34:273–281. [PubMed: 11308301]
27. Costentin C, Robert M, Savéant JM. Adiabatic and non-adiabatic concerted proton-electron transfers. Temperature effects in the oxidation of intramolecularly hydrogen-bonded phenols. J. Am. Chem. Soc. 2007; 129:9953–9963. [PubMed: 17637055]
28. Knapp MJ, Rickert K, Klinman JP. Temperature-dependent isotope effects in soybean lipoxygenase-1: correlating hydrogen tunneling with protein dynamics. J. Am. Chem. Soc. 2002; 124:3865–3874. [PubMed: 11942823]
29. Klinman JP. The role of tunneling in enzyme catalysis of C–H activation. Biochim. Biophys. Acta. 2006; 1757:981–987. [PubMed: 16546116]
30. Klinman JP. Linking protein structure and dynamics to catalysis: the role of hydrogen tunnelling. Philos. Trans. R. Soc. Lond. Ser. B. 2006; 361:1323–1331. [PubMed: 16873120]
31. Kuznetsov AM, Ulstrup J. Proton and hydrogen atom tunnelling in hydrolytic and redox enzyme catalysis. Can. J. Chem. 1999; 77:1085–1096.
32. Hatcher E, Soudackov AV, Hammes-Schiffer S. Proton-coupled electron transfer in soybean lipoxygenase: dynamical behavior and temperature dependence of kinetic isotope effects. J. Am. Chem. Soc. 2007; 129:187–196. [PubMed: 17199298]

33. Winkler JR, Nocera DG, Yocom KM, Bordignon E, Gray HB. Electron-transfer kinetics of pentaammineruthenium(III)(histidine-33)-ferricytochrome c. Measurement of the rate of intramolecular electron transfer between redox centers separated by 15 Å in a protein. J. Am. Chem. Soc. 1982; 104:5798–5800.
34. Nocera DG, Winkler JR, Yocom KM, Bordignon E, Gray HB. Kinetics of intermolecular and intramolecular electron transfer from ruthenium(II) complexes to ferricytochrome c. J. Am. Chem. Soc. 1984; 106:5145–5150.
35. Crane BR, Di Bilio AJ, Winkler JR, Gray HB. Electron tunneling in single crystals of *Pseudomonas aeruginosa* azurins. J. Am. Chem. Soc. 2001; 123:11623–11631. [PubMed: 11716717]
36. Beratan DN, Onuchic JN, Hopfield JJ. Electron tunneling through covalent and noncovalent pathways in proteins. J. Chem. Phys. 1987; 86:4488–4498.
37. Onuchic JN, Beratan DN. A predictive theoretical model for electron tunneling pathways in proteins. J. Chem. Phys. 1990; 92:722–733.
38. Beratan DN, Onuchic JN, Betts JN, Bowler BE, Gray HB. Electron tunneling pathways in ruthenated proteins. J. Am. Chem. Soc. 1990; 112:7915–7921.
39. Beratan DN, Betts JN, Onuchic JN. Protein electron transfer rates set by the bridging secondary and tertiary structure. Science. 1991; 252:1285–1288. [PubMed: 1656523]
40. Langen R, Chang IJ, Germanas JP, Richards JH, Winkler JR, Gray HB. Electron tunneling in proteins: coupling through a β strand. Science. 1995; 268:1733–1735. [PubMed: 7792598]
41. Turró C, Chang CK, Leroi GE, Cukier RI, Nocera DG. Photoinduced electron transfer mediated by a hydrogen-bonded interface. J. Am. Chem. Soc. 1992; 114:4013–4015.
42. Cukier RI. A theory that connects proton-coupled electron-transfer and hydrogen-atom transfer reactions. J. Phys. Chem. B. 2002; 106:1746–1757.
43. Zhao XG, Cukier RI. Molecular dynamics and quantum chemistry study of a proton-coupled electron transfer reaction. J. Phys. Chem. 1995; 99:945–954.
44. Sessler, JL.; Wang, B.; Springs, SL.; Brown, CT. Electron- and energy-transfer reactions in noncovalently linked supramolecular model systems. In: Murakami, Y., editor. Comprehensive Supramolecular Chemistry. Oxford: Pergamon; 1996. p. 311-336.
45. Ward MD. Photoinduced electron and energy transfer in non-covalently bonded supramolecular assemblies. Chem. Soc. Rev. 1997; 26:365–376.
46. Shafirovich VY, Courtney SH, Ya N, Geacintov NE. Proton-coupled photoinduced electron transfer, deuterium isotope effects, and fluorescence quenching in noncovalent benzo[a]pyrenetetraol-nucleoside complexes in aqueous solutions. J. Am. Chem. Soc. 1995; 117:4920–4929.
47. Ghaddar TH, Castner EW, Isied SS. Molecular recognition and electron transfer across a hydrogen bonding interface. J. Am. Chem. Soc. 2000; 122:1233–1234.
48. Roberts JA, Kirby JP, Nocera DG. Photoinduced electron transfer within a donor-acceptor pair juxtaposed by a salt bridge. J. Am. Chem. Soc. 1995; 117:8051–8052.
49. Kirby JP, van Dantzig NA, Chang CK, Nocera DG. Formation of porphyrin donor-acceptor complexes via an amidinium-carboxylate salt bridge. Tetrahedron Lett. 1995; 36:3477–3480.
50. Kirby JP, Roberts JA, Nocera DG. Significant effect of salt bridges on electron transfer. J. Am. Chem. Soc. 1997; 119:9230–9236.
51. Roberts JA, Kirby JP, Wall ST, Nocera DG. Electron transfer within ruthenium(II) polypyridyl-(salt bridge)-dimethylaniline acceptor-donor complexes. Inorg. Chim. Acta. 1997; 263:395–405.
52. Deng Y, Roberts JA, Peng SM, Chang CK, Nocera DG. The amidinium-carboxylate salt bridge as a proton-coupled interface to electron transfer pathways. Angew. Chem. Int. Ed. 1997; 36:2124–2127.
53. Soudackov A, Hammes-Schiffer S. Theoretical study of photoinduced proton-coupled electron transfer through asymmetric salt bridges. J. Am. Chem. Soc. 1999; 121:10598–10607.
54. Damrauer NH, Hodgkiss JM, Rosenthal J, Nocera DG. Observation of proton-coupled electron transfer by transient absorption spectroscopy in a hydrogen-bonded, porphyrin donor-acceptor assembly. J. Phys. Chem. B. 2004; 108:6315–6321. [PubMed: 18950117]

55. Rosenthal J, Hodgkiss JM, Young ER, Nocera DG. Spectroscopic determination of proton position in the proton-coupled electron transfer pathways of donor-acceptor supramolecule assemblies. J. Am. Chem. Soc. 2006; 128:10474–10483. [PubMed: 16895413]
56. Hodgkiss JM, Damrauer NH, Pressé S, Rosenthal J, Nocera DG. Temperature-isotope dependence reveals electron-transfer driven by proton-fluctuations in a hydrogen-bonded donor-acceptor assembly. J. Phys. Chem. B. 2006; 110:18853–18858. [PubMed: 16986876]
57. Cape JL, Bowman MK, Kramer DM. Reaction intermediates of quinol oxidation in a photoactivatable system that mimics electron transfer in the cytochrome bc_1 complex. J. Am. Chem. Soc. 2005; 127:4208–4215. [PubMed: 15783202]
58. Cha Y, Murray CJ, Klinman JP. Hydrogen tunneling in enzyme reactions. Science. 1989; 243:1325–1330. [PubMed: 2646716]
59. Dutton PL, Munro AW, Scrutton NS, Sutcliffe MJ. Introduction. Quantum catalysis in enzymes: beyond the transition state theory paradigm. Philos. Trans. R. Soc. Lond. Ser. B. 2006; 361:1293–1294.
60. Sutcliffe MJ, Masgrau L, Roujeinikova A, Johannissen LO, Hothi P, et al. Hydrogen tunnelling in enzyme-catalysed H-transfer reactions: flavoprotein and quinoprotein systems. Philos. Trans. R. Soc. Lond. Ser. B. 2006; 361:1375–1386. [PubMed: 16873125]
61. Klinman JP. Linking protein structure and dynamics to catalysis: the role of hydrogen tunneling. Philos. Trans. R. Soc. Lond. Ser. B. 2006; 361:1323–1331. [PubMed: 16873120]
62. Swain CG, Stivers EC, Reuwer JF, Schaad LJ. Use of hydrogen isotope effects to identify the attacking nucleophile in the enolization of ketones catalyzed by acetic acid. J. Am. Chem. Soc. 1958; 80:5885–5893.
63. Saunders WH. Calculations of isotope effects in elimination reactions. New experimental criteria for tunneling in slow proton transfers. J. Am. Chem. Soc. 1985; 107:164–169.
64. Glickman MH, Wiseman JS, Klinman JP. Extremely large isotope effects in the soybean lipoxygenase-linoleic acid reaction. J. Am. Chem. Soc. 1994; 116:793–794.
65. Glickman MH, Cliff S, Thiemens M, Klinman JP. Comparative study of ^{17}O and ^{18}O isotope effects as a probe for dioxygen activation: application to the soybean lipoxygenase reaction. J. Am. Chem. Soc. 1997; 119:11357–11361.
66. Rickert KW, Klinman JP. Nature of hydrogen transfer in soybean lipoxygenase 1: separation of primary and secondary isotope effects. Biochemistry. 1999; 38:12218–12228. [PubMed: 10493789]
67. Fischer E. Einfluss der Configuration auf die Wirkung der Enzyme. Ber. Deut. Chem. Ges. 1894; 27:2985–2993.
68. Koshland DE. Application of a theory of enzyme specificity to protein synthesis. Proc. Natl. Acad. Sci. USA. 1958; 44:98–104. [PubMed: 16590179]
69. Roth JP, Mayer JM. Hydrogen transfer reactivity of a ferric bi-imidazoline complex that models the activity of lipoxygenase enzymes. Inorg. Chem. 1999; 38:2760–2761. [PubMed: 11671018]
70. Roth JP, Lovell S, Mayer JM. Intrinsic barriers for electron and hydrogen atom transfer reactions of biomimetic iron complexes. J. Am. Chem. Soc. 2000; 122:5486–5498.
71. Hodgkiss, JM.; Rosenthal, J.; Nocera, DG. The relation between hydrogen atom transfer and proton-coupled electron transfer in model systems. In: Hynes, JT.; Klinman, JP.; Limbach, H-H.; Schowen, RL., editors. Handbook of Hydrogen Transfer. Physical and Chemical Aspects of Hydrogen Transfer. Weinheim, Ger.: Wiley-VCH; 2006. p. 503-562.
72. Stubbe J, van der Donk WA. Protein radicals in enzyme catalysis. Chem. Rev. 1998; 98:705–762. [PubMed: 11848913]
73. Whittaker JW. Free radical catalysis by galactose oxidase. Chem. Rev. 2003; 103:2347–2364. [PubMed: 12797833]
74. Frey PA, Hegeman AD, Reed GH. Free radical mechanisms in enzymology. Chem. Rev. 2006; 106:3302–3316. [PubMed: 16895329]
75. Stubbe J, Nocera DG, Yee CS, Chang MCY. Radical initiation in the class I ribonucleotide reductase: Long-range proton-coupled electron transfer? Chem. Rev. 2003; 103:2167–2202. [PubMed: 12797828]

76. Meyer TJ, Huynh MHV, Thorp HH. The possible role of proton-coupled electron transfer (PCET) in water oxidation by photosystem II. Angew. Chem. Int. Ed. 2007; 46:5284–5304.
77. Sjödin M, Styring S, Wolpher H, Xu Y, Sun L, Hammarström L. Switching the redox mechanism: models for proton-coupled electron transfer from tyrosine and tryptophan. J. Am. Chem. Soc. 2005; 127:3855–3863. [PubMed: 15771521]
78. Voet, D.; Voet, JG. Biochemistry. New York: Wiley; 1995.
79. Durrant JR, Klug DR, Kwa SLS, Grondelle RV, Porter G, Dekker JP. A multimer model for P680, the primary electron donor of photosystem II. Proc. Natl. Acad. Sci. USA. 1995; 92:4798–4802. [PubMed: 11607546]
80. Paddock ML, Feher G, Okamura MY. Proton transfer pathways and mechanism in bacterial reaction centers. FEBS Lett. 2003; 555:45–50. [PubMed: 14630317]
81. Kok B, Forbush B, McGloin M. Cooperation of charges in photosynthetic O_2 evolution-I. A linear four step mechanism. Photochem. Photobiol. 1970; 11:457–475. [PubMed: 5456273]
82. Forbush B, Kok B, McGloin M. Cooperation of charges in photosynthetic oxygen evolution. II. Damping of flash yield oscillation, deactivation. Photochem. Photobiol. 1971; 14:307–321.
83. McEvoy JP, Brudvig GW. Water-splitting chemistry of photosystem II. Chem. Rev. 2006; 106:4455–4483. [PubMed: 17091926]
84. Haumann M, Liebisch P, Muller C, Barra M, Grabolle M, Dau H. Photosynthetic O_2 formation tracked by time-resolved X-ray experiments. Science. 2005; 310:1019–1021. [PubMed: 16284178]
85. Barry BA, Babcock GT. Tyrosine radicals are involved in the photosynthetic oxygen-evolving system. Proc. Natl. Acad. Sci. USA. 1987; 84:7099–7103. [PubMed: 3313386]
86. Debus RJ, Barry BA, Babcock GT, McIntosh L. Site-directed mutagenesis identifies a tyrosine radical involved in the photosynthetic oxygen-evolving system. Proc. Natl. Acad. Sci. USA. 1988; 85:427–430. [PubMed: 2829186]
87. Debus RJ, Barry BA, Sithole I, Babcock GT, McIntosh L. Directed mutagenesis indicates that the donor to P 680+ in photosystem II is tyrosine-161 of the D1 polypeptide. Biochemistry. 1988; 27:9071–9074. [PubMed: 3149511]
88. Diner BA, Nixon PJ, Farchaus JW. Site-directed mutagenesis of photosynthetic reaction centers. Curr. Opin. Struct. Biol. 1991; 1:546–554.
89. Chu H-A, Nguyen AP, Debus RJ. Amino acid residues that influence the binding of manganese or calcium to photosystem II. 1. The lumenal interhelical domains of the D1 polypeptide. Biochemistry. 1995; 34:5839–5858. [PubMed: 7727445]
90. Hoganson CW, Babcock GT. A metalloradical mechanism for the generation of oxygen from water in photosynthesis. Science. 1997; 277:1953–1956. [PubMed: 9302282]
91. Hays AMA, Vassiliev IR, Golbeck JH, Debus RJ. Role of D1-His190 in proton-coupled electron transfer reactions in photosystem II: a chemical complementation study. Biochemistry. 1998; 37:11352–11365. [PubMed: 9698383]
92. Diner BA, Force DA, Randall DW, Britt RD. Hydrogen bonding, solvent exchange, and coupled proton and electron transfer in the oxidation and reduction of redox-active tyrosine Y_Z in Mn-depleted core complexes of photosystem II. Biochemistry. 1998; 37:17931–17943. [PubMed: 9922161]
93. Loll B, Kern J, Saenger W, Zouni A, Biesiadka J. Towards complete cofactor arrangement in the 3.0 Å resolution structure of photosystem II. Nature. 2005; 438:1040–1044. [PubMed: 16355230]
94. Jordan A, Reichard P. Ribonucleotide reductases. Annu. Rev. Biochem. 1998; 67:71–98. [PubMed: 9759483]
95. Stubbe J. Radicals with a controlled lifestyle. Chem. Comm. Oct. 2003; (20):2511–2513.
96. Thelander L. Physicochemical characterization of ribonucleoside diphosphate reductase from *Escherichia coli*. J. Biol. Chem. 1973; 248:4591–4601. [PubMed: 4578086]
97. Kashlan OB, Scott CP, Lear JD, Cooperman BS. A comprehensive model for the allosteric regulation of mammalian ribonucleotide reductase. Functional consequences of ATP- and dATP-induced oligomerization of the large subunit. Biochemistry. 2002; 41:462–474. [PubMed: 11781084]

98. Kashlan OB, Cooperman BS. Comprehensive model for allosteric regulation of mammalian ribonucleotide reductase: refinements and consequences. Biochemistry. 2003; 42:1696–1706. [PubMed: 12578384]

99. Stubbe J, Riggs-Gelasco P. Harnessing free radicals: formation and function of the tyrosyl radical in ribonucleotide reductase. Trends Biochem. Sci. 1998; 23:438–443. [PubMed: 9852763]

100. Uhlin U, Eklund H. Structure of ribonucleotide reductase protein R1. Nature. 1994; 370:533–539. [PubMed: 8052308]

101. Nordlund P, Sjöberg B-M, Eklund H. Three-dimensional structure of the free radical protein of ribonucleotide reductase. Nature. 1990; 345:593–598. [PubMed: 2190093]

102. Högbom M, Galander M, Andersson M, Kolberg M, Hofbauer W, et al. Displacement of the tyrosyl radical cofactor in ribonucleotide reductase obtained by single-crystal high-field EPR and 1.4-Å X-ray data. Proc. Natl. Acad. Sci. USA. 2003; 100:3209–3214. [PubMed: 12624184]

103. Bennati M, Robblee JH, Mugnaini V, Stubbe J, Freed JH, Borbat P. EPR distance measurements support a model for long-range radical initiation in *E. coli* ribonucleotide reductase. J. Am. Chem. Soc. 2005; 127:15014–15015. [PubMed: 16248626]

104. Ekberg M, Potsch S, Sandin E, Thunnissen M, Nordlund P, et al. Preserved catalytic activity in an engineered ribonucleotide reductase R2 protein with a nonphysiological radical transfer pathway. The importance of hydrogen bond connections between the participating residues. J. Biol. Chem. 1998; 273:21003–21008. [PubMed: 9694851]

105. Ekberg M, Sahlin M, Eriksson M, Sjöberg B-M. Two conserved tyrosine residues in protein R1 participate in an intermolecular electron transfer in ribonucleotide reductase. J. Biol. Chem. 1996; 271:20655–20659. [PubMed: 8702814]

106. Rova U, Goodtzova K, Ingemarson R, Behravan G, Graeslund A, Thelander L. Evidence by site-directed mutagenesis supports long-range electron transfer in mouse ribonucleotide reductase. Biochemistry. 1995; 34:4267–4275. [PubMed: 7703240]

107. Rova U, Adrait A, Potsch S, Graslund A, Thelander L. Evidence by mutagenesis that Tyr370 of the mouse ribonucleotide reductase R2 protein is the connecting link in the intersubunit radical transfer pathway. J. Biol. Chem. 1999; 274:23746–23751. [PubMed: 10446134]

108. Ge J, Yu G, Ator MA, Stubbe J. Pre-steady-state and steady-state kinetic analysis of *E. coli* class I ribonucleotide reductase. Biochemistry. 2003; 42:10071–10083. [PubMed: 12939135]

109. Yee CS, Seyedsayamdost MR, Chang MCY, Nocera DG, Stubbe J. Generation of the R2 subunit of ribonucleotide reductase by intein chemistry: insertion of 3-nitrotyrosine at residue 356 as a probe of the radical initiation process. Biochemistry. 2003; 42:14541–14552. [PubMed: 14661967]

110. Yee CS, Chang MCY, Ge J, Nocera DG, Stubbe J. 2,3-Difluorotyrosine at position 356 of ribonucleotide reductase R2: a probe of long-range proton-coupled electron transfer. J. Am. Chem. Soc. 2003; 125:10506–10507. [PubMed: 12940718]

111. Chang MCY, Yee CS, Nocera DG, Stubbe J. Site-specific replacement of a conserved tyrosine in ribonucleotide reductase with an aniline amino acid: a mechanistic probe for a redox-active tyrosine. J. Am. Chem. Soc. 2004; 126:16702–16703. [PubMed: 15612690]

112. Seyedsayamdost MR, Yee CS, Reece SY, Nocera DG, Stubbe J. pH rate profiles of F_nY_{356}-R2s (n = 2, 3, 4) in *Escherichia coli* ribonucleotide reductase: evidence that Y_{356} is a redox-active amino acid along the radical propagation pathway. J. Am. Chem. Soc. 2006; 128:1562–1568. [PubMed: 16448127]

113. Seyedsayamdost MR, Reece SY, Nocera DG, Stubbe J. Mono-, di-, tri-, and tetra-substituted fluorotyrosines: new probes for enzymes that use tyrosyl radicals in catalysis. J. Am. Chem. Soc. 2006; 128:1569–1579. [PubMed: 16448128]

114. Xie J, Schultz PG. A chemical toolkit for proteins—an expanded genetic code. Nat. Rev. Mol. Cell Biol. 2006; 7:775–782. [PubMed: 16926858]

115. Seyedsayamdost MR, Xie J, Chan CTY, Schultz PG, Stubbe J. Site-specific insertion of 3-aminotyrosine into subunit α2 of *E. coli* ribonucleotide reductase: direct evidence for involvement of Y730 and Y731 in radical propagation. J. Am. Chem. Soc. 2007; 129:15060–15071. [PubMed: 17990884]

116. Reece, SY.; Nocera, DG. Proton-coupled electron transfer: the engine that drives radical transport and catalysisin biology. In: Scrutton, NS.; Alleman, R., editors. Quantum Tunneling in Enzyme-Catalyzed Reactions. Cambridge, UK: R. Soc. Chem.; 2009. p. 351-383.

117. Climent I, Sjöberg BM, Huang CY. Carboxyl-terminal peptides as probes for *Escherichia coli* ribonucleotide reductase subunit interaction: kinetic analysis of inhibition studies. Biochemistry. 1991; 30:5164–5171. [PubMed: 2036382]

118. Climent I, Sjöberg BM, Huang CY. Site-directed mutagenesis and deletion of the carboxyl terminus of *Escherichia coli* ribonucleotide reductase protein R2. Effects on catalytic activity and subunit interaction. Biochemistry. 1992; 31:4801–4807. [PubMed: 1591241]

119. Chang MCY, Yee CS, Stubbe J, Nocera DG. Turning on ribonucleotide reductase by light-initiated amino acid radical generation. Proc. Natl. Acad. Sci. USA. 2004; 101:6882–6887. [PubMed: 15123822]

120. Reece SY, Seyedsayamdost MR, Stubbe J, Nocera DG. Photoactive peptides for light-initiated tyrosyl radical generation and transport into ribonucleotide reductase. J. Am. Chem. Soc. 2007; 129:8500–8509. [PubMed: 17567129]

121. Reece SY, Seyedsayamdost MR, Stubbe J, Nocera DG. Direct observation of a transient tyrosine radical competent for initiating turnover in a photochemical ribonucleotide reductase. J. Am. Chem. Soc. 2007; 129:13828–13830. [PubMed: 17944464]

122. Sjödin M, Styring S, Åkermark B, Sun L, Hammarström L. Proton-coupled electron transfer from tyrosine in a tyrosine-ruthenium-tris-bipyridine complex: comparison with tyrosineZ oxidation in photosystem II. J. Am. Chem. Soc. 2000; 122:3932–3936.

123. Reece SY, Nocera DG. Direct tyrosine oxidation using the MLCT excited states of rhenium polypyridyl complexes. J. Am. Chem. Soc. 2005; 127:9448–9458. [PubMed: 15984872]

124. Fecenko CJ, Meyer TJ, Thorp HH. Electrocatalytic oxidation of tyrosine by parallel rate-limiting proton transfer and multisite electron-proton transfer. J. Am. Chem. Soc. 2006; 128:11020–11021. [PubMed: 16925408]

125. Costentin C, Robert M, Savéant JM. Concerted proton-electron transfer reactions in water. Are the driving force and rate constant depending on pH when water acts as proton donor or acceptor? J. Am. Chem. Soc. 2007; 129:5870–5879. [PubMed: 17428051]

126. Irebo T, Reece SY, Sjödin M, Nocera DG, Hammarström L. Proton-coupled electron transfer of tyrosine oxidation: buffer dependence and parallel mechanisms. J. Am. Chem. Soc. 2007; 129:15462–15464. [PubMed: 18027937]

127. Tommos C, Skalicky JJ, Pilloud DL, Wand AJ, Dutton PL. De novo proteins as models of radical enzymes. Biochemistry. 1999; 38:9495–9507. [PubMed: 10413527]

128. Ishikita H, Soudackov AV, Hammes-Schiffer S. Buffer-assisted proton-coupled electron transfer in a model rhenium-tyrosine complex. J. Am. Chem. Soc. 2007; 129:11146–11152. [PubMed: 17705482]

129. Costentin C, Robert M, Savéant JM. Electrochemical and homogeneous proton-coupled electron transfers: concerted pathways in the one-electron oxidation of a phenol coupled with an intramolecular amine-driven proton transfer. J. Am. Chem. Soc. 2006; 128:4552–4553. [PubMed: 16594674]

130. Rhile IJ, Mayer JM. One-electron oxidation of a hydrogen-bonded phenol occurs by concerted proton-coupled electron transfer. J. Am. Chem. Soc. 2004; 126:12718–12719. [PubMed: 15469234]

131. Rhile IJ, Markle TF, Nagao H, DiPasquale AG, Lam OP, et al. Concerted proton-electron transfer in the oxidation of hydrogen-bonded phenols. J. Am. Chem. Soc. 2006; 128:6075–6088. [PubMed: 16669677]

132. Suydam IT, Snow CD, Pande VS, Boxer SG. Electric fields at the active site of an enzyme: direct comparison of experiment with theory. Science. 2006; 313:200–204. [PubMed: 16840693]

133. Sjödin M, Irebo T, Utas JE, Lind J, Merényi G, et al. Kinetic effects of hydrogen bonds on proton-coupled electron transfer from phenols. J. Am. Chem. Soc. 2006; 128:13076–13083. [PubMed: 17017787]

134. Costentin C, Evans DH, Robert M, Savéant JM, Singh PS. Electrochemical approach to concerted proton and electron transfers. Reduction of the water-superoxide ion complex. J. Am. Chem. Soc. 2005; 127:12490–12491. [PubMed: 16144387]

SUMMARY POINTS

1. Proton-coupled electron transfer (PCET) may occur along unidirectional and bidirectional pathways with concerted or stepwise mechanisms.
2. The proton will affect electron transport even if the electron and proton do not move together. Furthermore, the same electron and proton do not have to couple throughout an entire biological transformation.
3. Biology has developed elaborate structural motifs to preserve coupling of the electron and proton, despite the fact that the electron and proton tunnel on very different length scales.
4. PCET is involved in the transfer of an electron through hydrogen bonds. Although hydrogen bonds are effective coupling mediums for electron transfer (ET), the rate of ET is impeded compared to covalent bonds by approximately a factor of 4.The electronic coupling may be a dynamic factor influenced by thermal fluctuations of the proton within the hydrogen-bonded interface.
5. The PCET activation of the C–H bonds of substrates by metallocofactors fundamentally differs from classical hydrogen atom transfer reactions. In the latter, the electron and proton are transferred from one bond to another. In biology, the electron and proton originate from the same bond, but they are transferred to different sites, the electron to the metal of the cofactor and the proton to a ligand.
6. Oxidation of tyrosine may proceed via a host of mechanisms depending upon the oxidant strength and may be facilitated by concerted proton transfer (PT) to a hydrogen-bonded base.
7. For enzymatic reactions that utilize $Y^{\bullet}$, radical transport by a PCET mechanism does not demand that the proton be obligated to the electron, although PCET prevails at the terminus of the network.
8. PCET provides biology with an exquisite mechanism for achieving substrate selectivity owing to the considerable sensitivity of proton tunneling to distance.

FUTURE ISSUES

1. Direct kinetics measurements of PCET in biological and model systems to date have primarily focused on detecting the ET kinetics component of the transformation. Insight into PCET reaction mechanisms will be expanded considerably with experimental optical and vibrational methods that directly probe the kinetics of the PT component of the reaction in addition to the ET component.
2. The continued discovery of unnatural amino acids that permit radical PCET to be triggered for amino acid radicals in addition to tyrosine (especially glycine and tryptophan) will permit the greater scope of enzyme function to be defined.
3. New PCET theories need to be developed that are predictive of kinetics, in much the same way that Marcus theory is for ET. Such theories will be useful for the design of enzyme function and will provide tests of fundamental issues surrounding PCET, such as whether the Born-Oppenheimer approximation is valid for describing a PCET reaction.
4. Model systems need to be developed that allow the proton and electron to be orthog-onalized so that the proton and electron transfer distances and driving forces may be independently controlled. These systems will allow the kinetic isotope effect (KIE) for a PCET reaction to be measured as a function of the tunneling distance for the proton.
5. Temperature-dependent KIE measurements will effectively probe the dynamic nature of electronic coupling during PCET.
6. Measurement of PCET reactions with two-dimensional optical and vibrational spectro-scopies will permit the direct measurement of the nuclear modes by which the electron and proton couple.
7. The theoretical and experimental framework for developing how an electron couples to a proton needs to be expanded to treat atoms that are heavier than the proton. The most important heavy atoms for biological energy conversion are carbon, nitrogen, and oxygen.

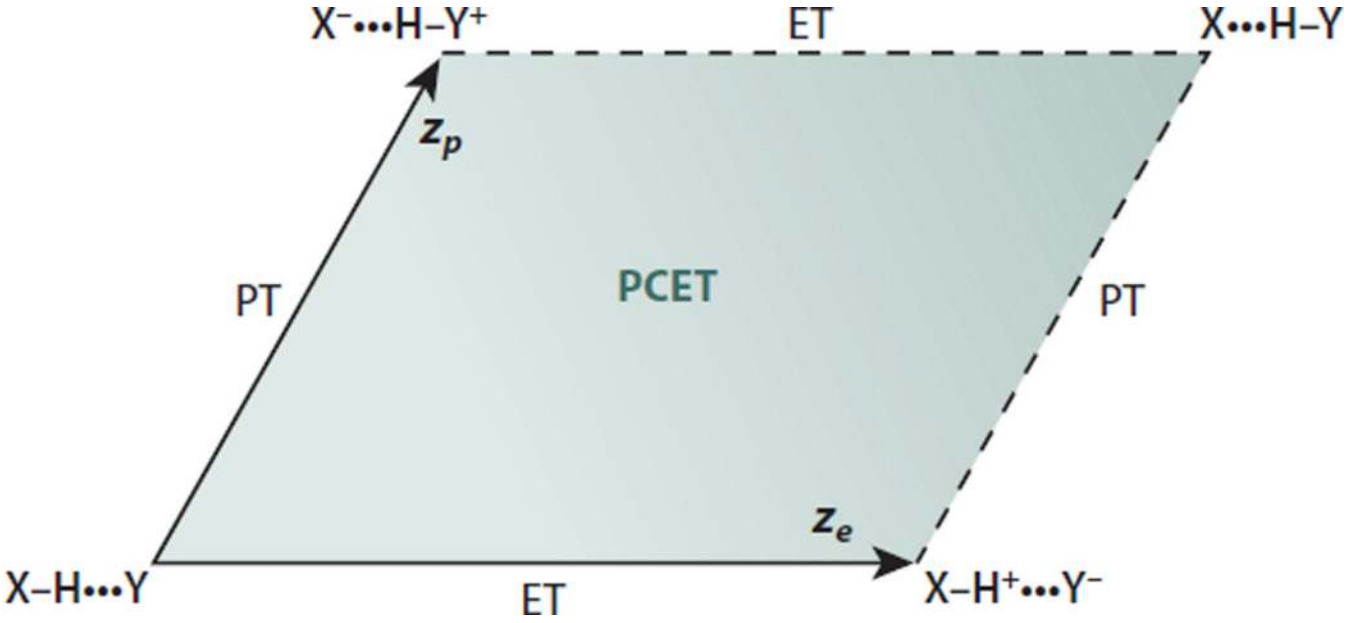

Figure 1.
Scheme for proton-coupled electron transfer (PCET). X is the electron transfer (ET) and proton transfer (PT) donor, and Y is the acceptor.

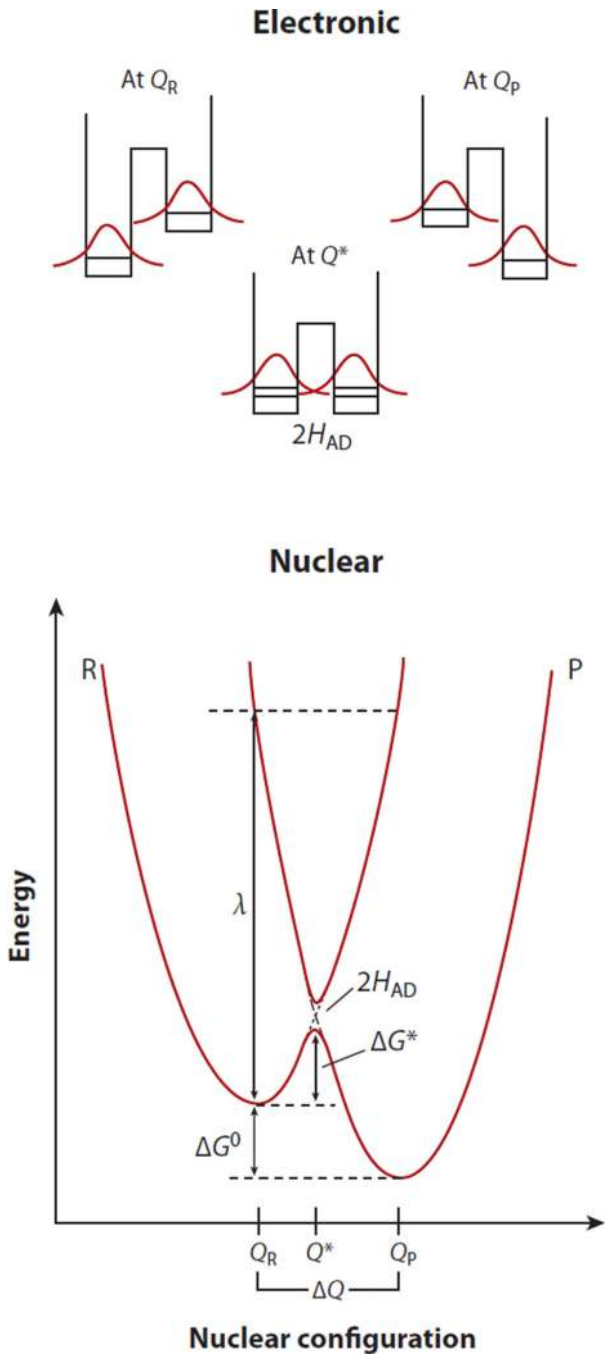

Figure 2.

Potential energy well for an electron transfer reaction treated quantum mechanically. R and P are the reactant and product vibrational energy well, respectively. $\Delta G°$ and ΔG^* are the free energies of reaction and activation, λ represents the total reorganization energy, and H_{AD} is the electronic coupling between acceptor and donor. Q^* is the coordinate of interest to the system at the transition state.

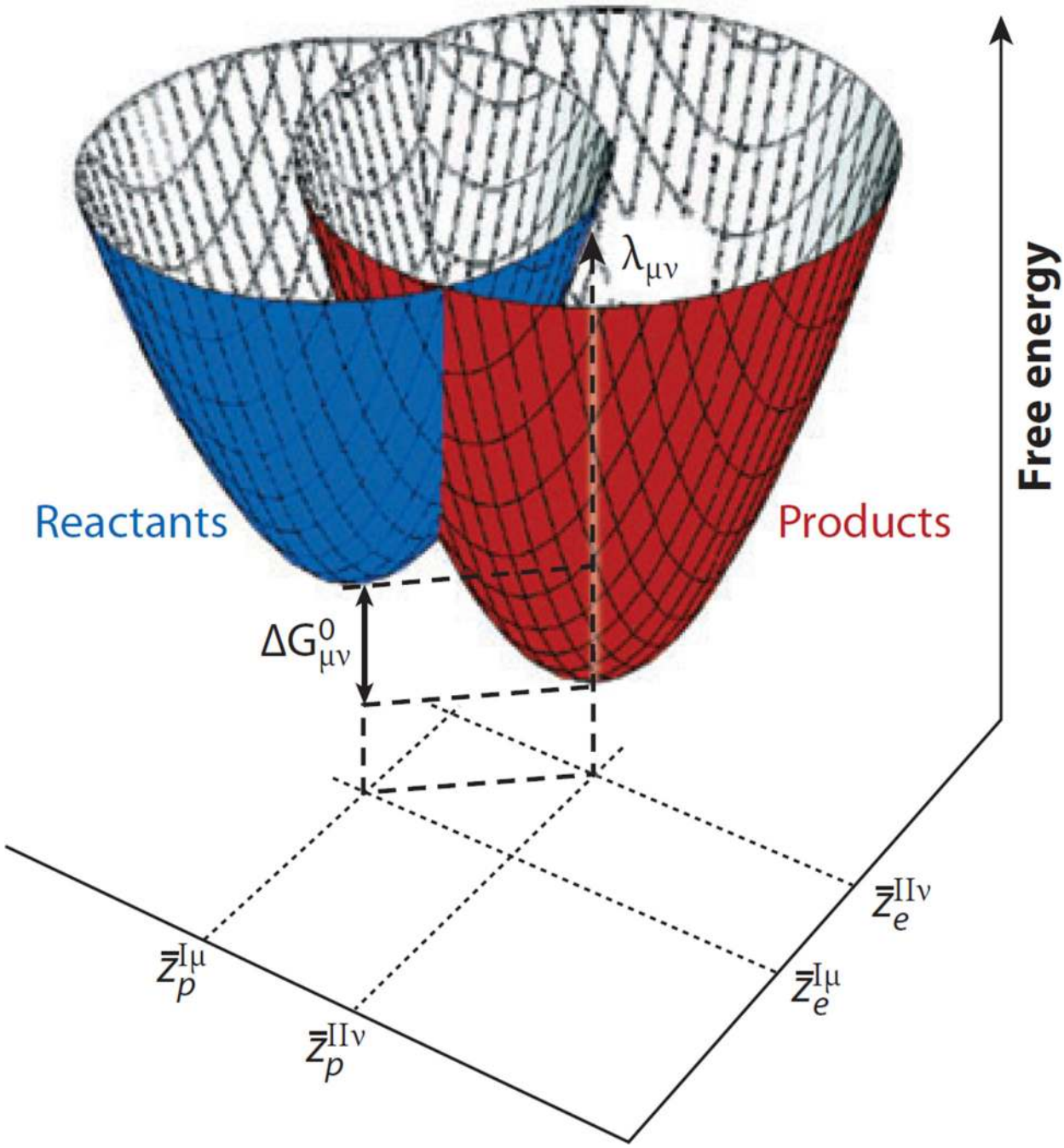

Figure 3.
Three dimensional vibronic free-energy surfaces for reactants, I, μ (*blue*), and products, II, *v*(*red*), of a proton-coupled electron transfer reaction. From Reference 13.

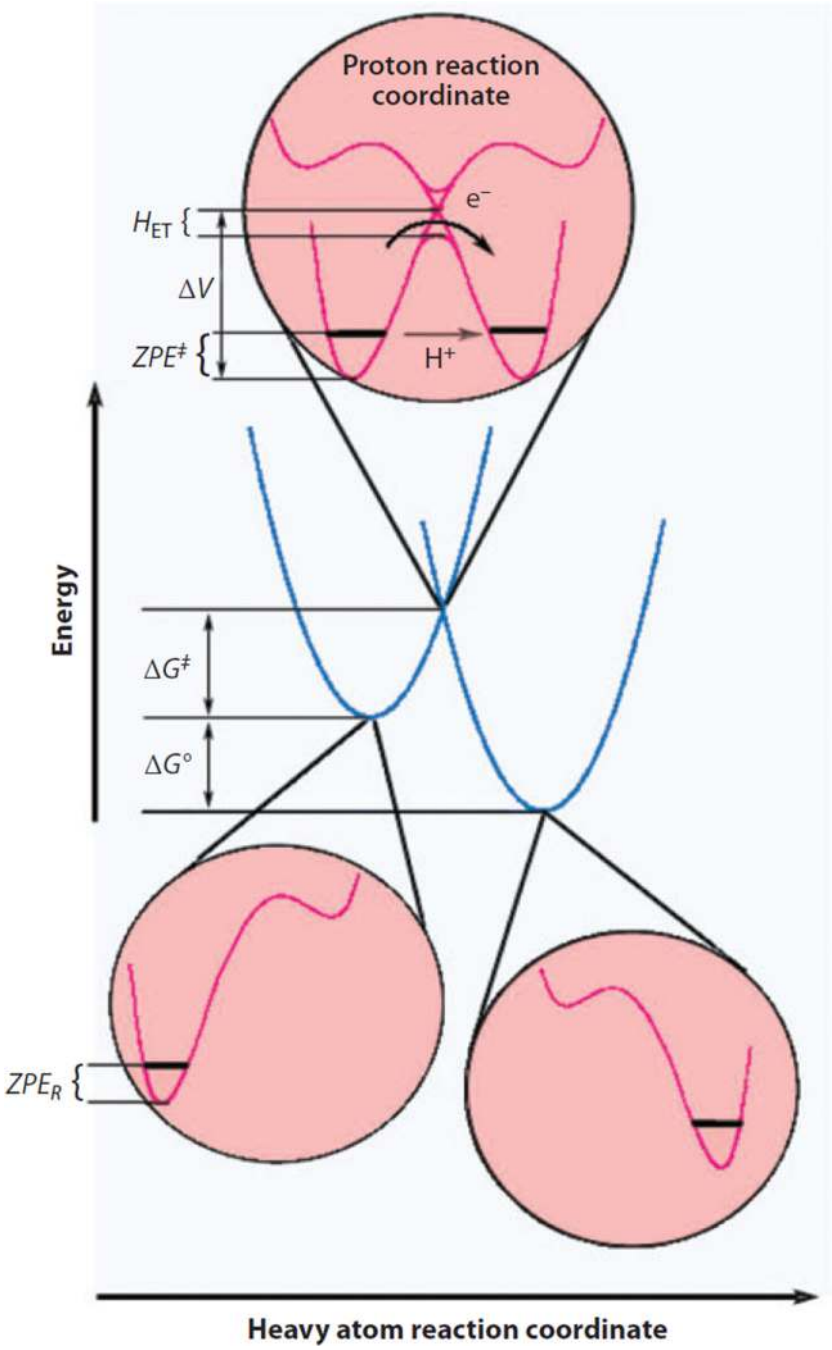

Figure 4.

Two-dimensional potential energy profiles for a concerted proton-coupled electron transfer reaction. The circles (*pink*) represent the vibrational energy surface for the transferring hydrogen atom at the lowest energy of the reactant and product well and at the transition state. Note that optimal overlap occurs at the reaction transition state where the lowest energy of the H-vibrational wavefunction is the same in the reactant and product well. From Reference 27.

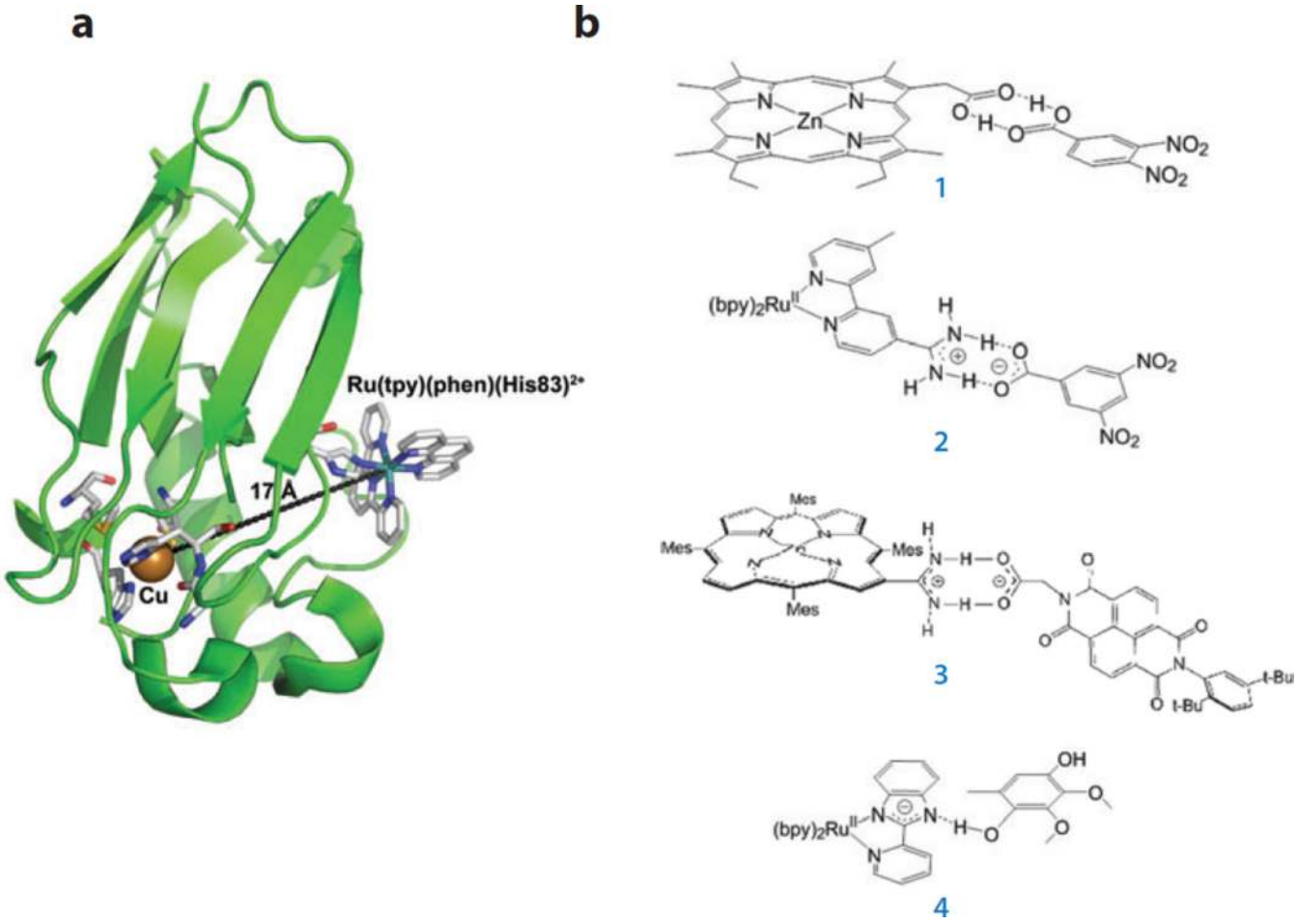

Figure 5.

Biological and model systems for examination of the role of the proton in electron transfer (ET) in proteins. (*a*) X-ray crystal structure of *Pseudomonas aeruginosa* oxidized azurin(Cu^{2+}) with Ru(tpy)(phen)(His83)$^{2+}$ label. Data from Reference 35, Protein Data Bank (PDB) code 1JZE. (*b*) Model systems developed to examine the role of the proton in mediating ET through hydrogen-bonded networks (54, 56). Numbers identify the compounds in the text.

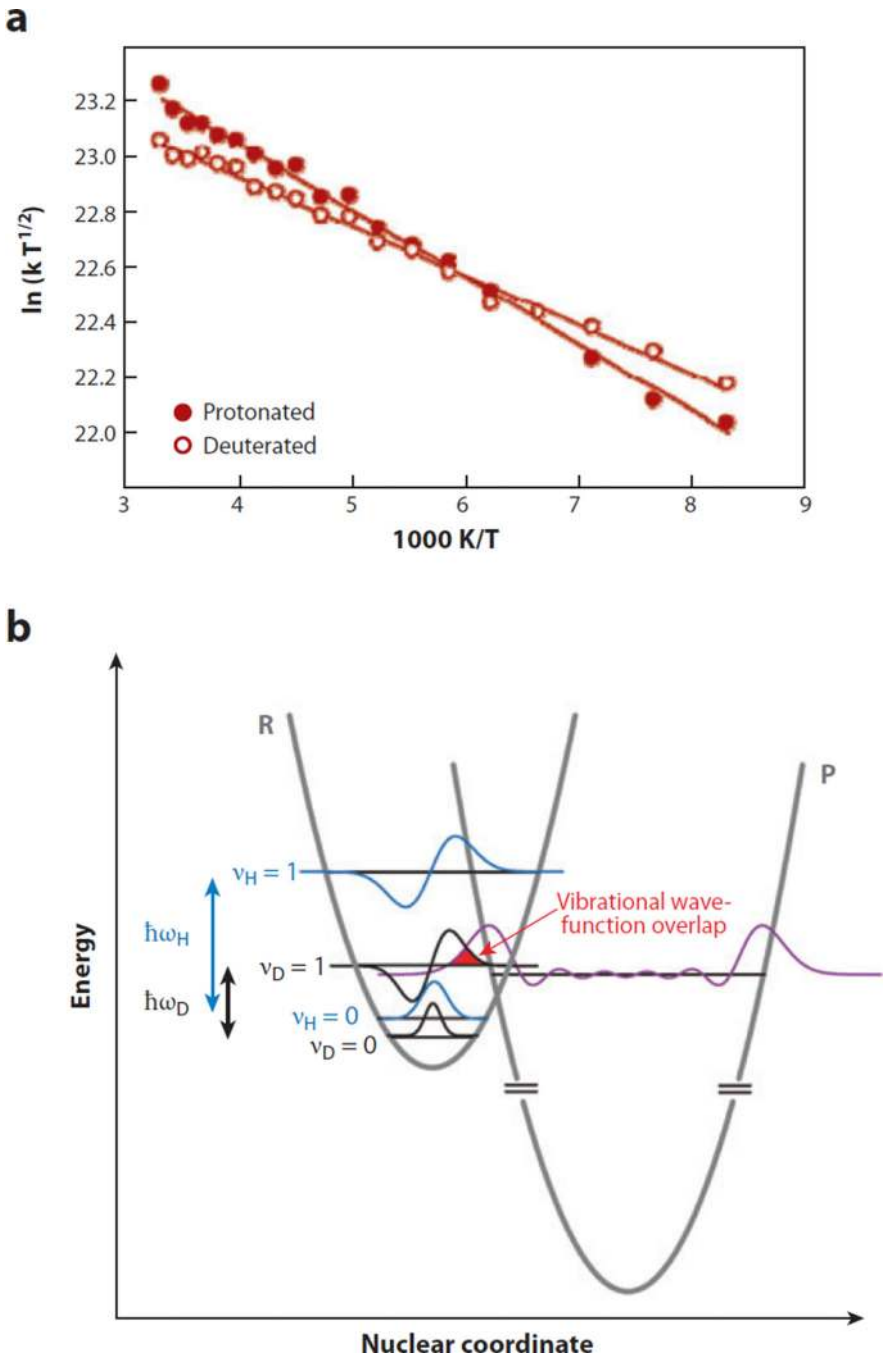

Figure 6.

(*a*) T dependency of the rate of proton-coupled electron transfer in assembly **3** with a protonated (*solid circles*) and deuterated (*open circles*) in the solvent 2-methyltetrahydrofuran. (*b*) Model for interpretation of the inverted kinetic isotope effect. Proton and deuteron ground ($v = 0$) and excited-state ($v = 1$) reactant vibrational wavefunctions are illustrated in blue and black, respectively. Proton vibrational energies ($\hbar\omega$) are greater than that for the deuteron. A vibrational wavefunction for the product well

is illustrated in magenta. Vibrational wavefunction overlap (*red*) facilitates electron tunneling from the reactant (R) to the product (P) well.

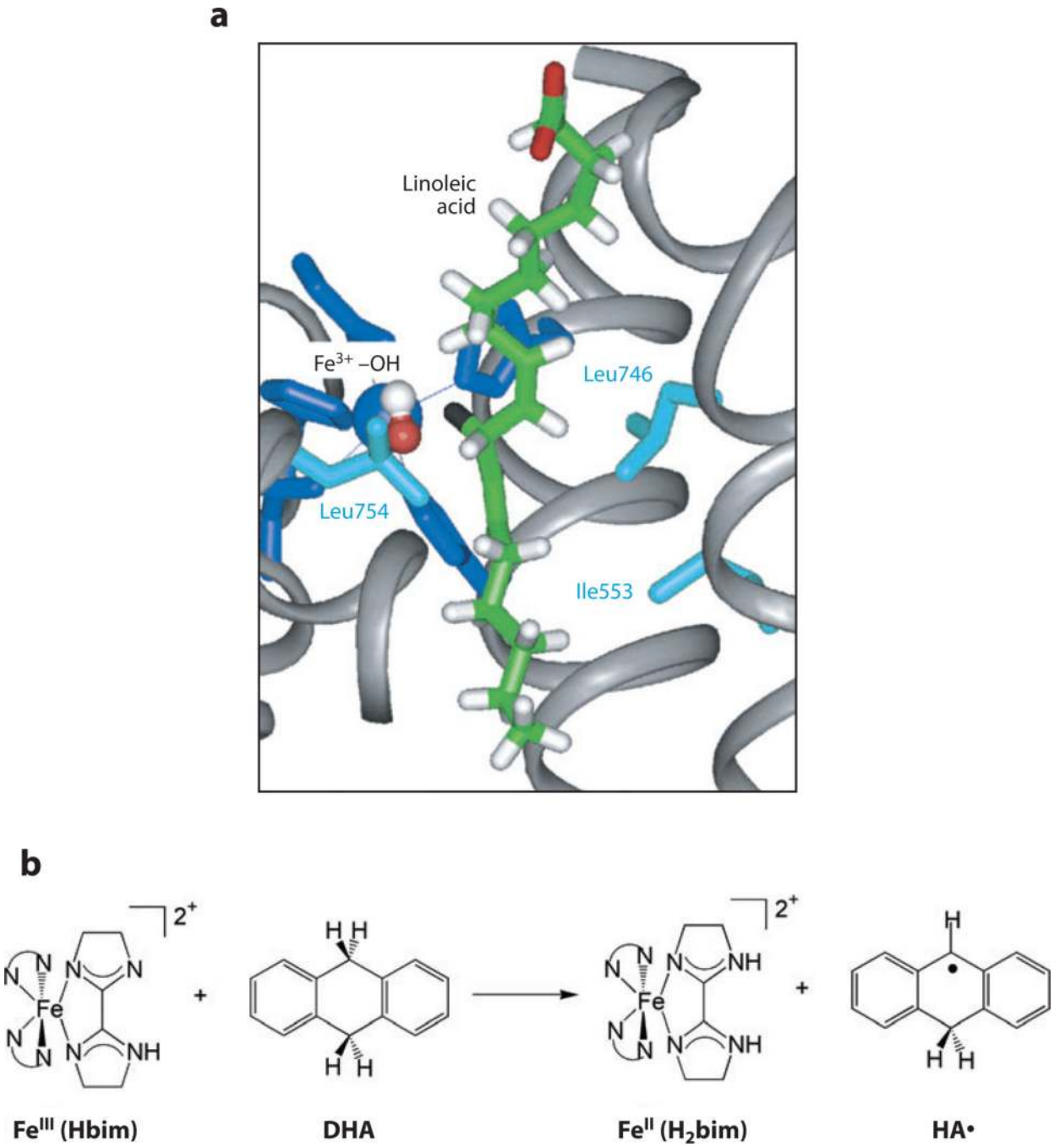

Figure 7.

Biological and model systems for examination of the role of PCET in C–H activation of substrates: (*a*) Model of linoleic acid (LA) in the crystal structure of soybean lipoxygenase-1 (SLO). Fe^{3+} and its protein-derived ligands (*dark blue*); the hydroxo-ligand (red/white); LA (*green/red/white*), with the pro-S hydrogen (*black*) of C-11; and Leu546, Leu754, and Ile553 (*light blue*) are illustrated. From Reference 28. (*b*) The concerted proton-coupled electron transfer reaction of Fe^{III}(Hbim) with dihydroanthracene (DHA), which models the C–H activation reaction of SLO.

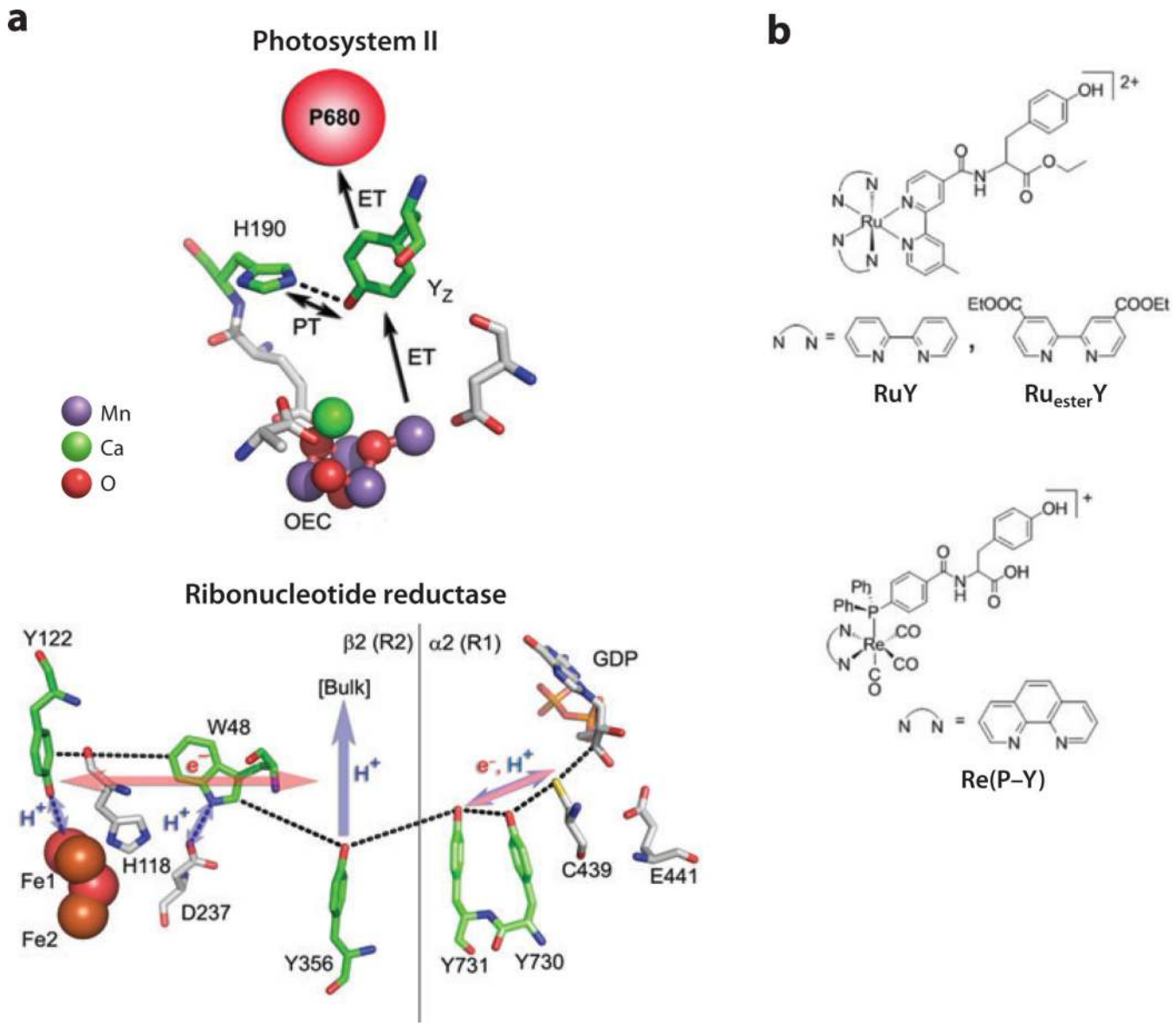

Figure 8.

Biological and model systems for examination of the proton-coupled electron transfer (PCET) mechanism of tyrosine radical generation and transport: (*a*) (*top*) Crystal structure of photosystem II–oxidizing cofactors (93). Purple and green spheres represent a model for electron density corresponding to Mn and Ca, respectively, in the oxygen-evolving complex (OEC) and red sphere represents O. PDB code: 2AXT. (*bottom*) Conserved residues of class I ribonucleotide reductase that compose the putative PCET pathway for radical transport from •Y122 in β2 to C439 in the α2 active site (100, 102). Residues where the radical has been directly observed or trapped via site-specific replacement with nonnatural amino acid analogs are green. Y356 is not located in either the β2 or α2 crystal structures. (*b*) Structures of model complexes RuY, $Ru_{ester}Y$, and Re(P–Y) discussed herein for the study of PCET mechanisms of Y oxidation.

Unidirectional PCET

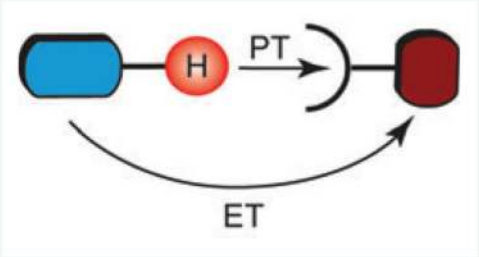

Concerted electron-proton transfer (CEP) (133)
Electron-proton transfer (EPT) (26, 76)
Concerted proton-electron transfer (CPET) (131, 134)
Concerted electron transfer proton transfer (ETPT) (42)

Bidirectional PCET

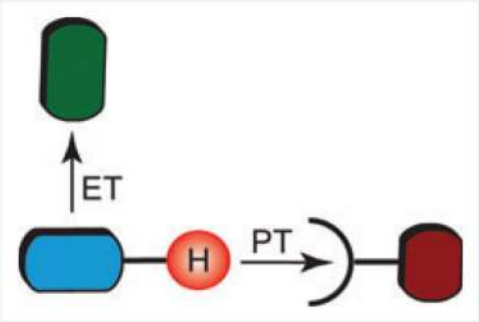

Bidirectional concerted electron-proton transfer (CEP) (133)
Multisite electron proton transfer (MS-EPT) (76)

Scheme 1.
The language of proton-coupled electron transfer (PCET). Abbreviations: ET, electron transfer; PT, proton transfer. The numbers in parentheses correspond to references listed in the Literature Cited section.

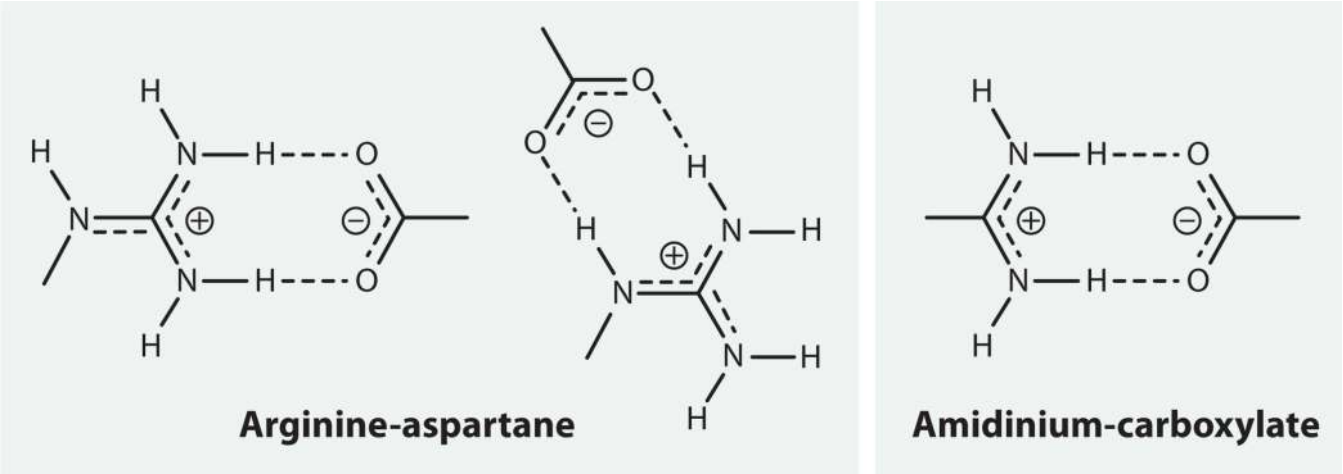

Scheme 2.

The guanidinium of an Arg-Asp salt bridge can assume multiple two-point binding conformations; only one two-point conformation may be assumed upon replacing guanidinium with amidinium.

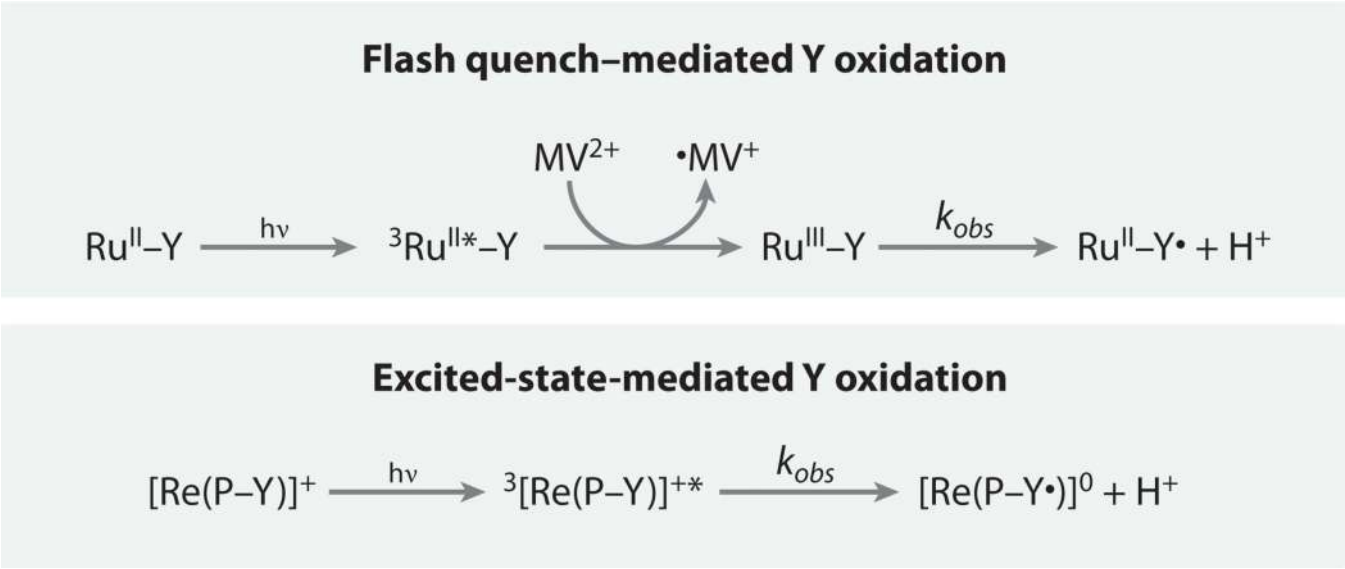

Scheme 3.
Mechanisms of $Y^{\bullet}$ generation employed in model complexes discussed herein.